



# Mineral potential modelling of orogenic gold systems in the granites-tanami Orogen, Northern Territory, Australia: A multi-technique approach

Bijan Roshanravan<sup>a</sup>, Oliver P. Kreuzer<sup>b,c,\*</sup>, Amanda Buckingham<sup>d,e</sup>,  
Majid Keykhay-Hosseini<sup>a,f</sup>, Edward Keys<sup>g</sup>

<sup>a</sup> Department of Mining Engineering, Faculty of Engineering, University of Birjand, Birjand, Iran

<sup>b</sup> Corporate Geoscience Group (CGSG), PO Box 5128, Rockingham Beach, WA 6969, Australia

<sup>c</sup> Economic Geology Research Centre (EGRU), College of Science & Engineering, James Cook University, Townsville, QLD 4811, Australia

<sup>d</sup> Fathom Geophysics Australia, PO Box 1253, Dunsborough, WA 6281, Australia

<sup>e</sup> Centre of Exploration Targeting (CET), The University of Western Australia, 35 Stirling Highway, Crawley, WA 6009, Australia

<sup>f</sup> Center of Studies in Resource Engineering, Indian Institute of Technology Bombay, Mumbai, India

<sup>g</sup> Prodigy Gold NL, Level 1, 141 Broadway, Nedlands, WA 6009, Australia

## ARTICLE INFO

### Keywords:

Granites-tanami orogen  
Gold  
Targeting  
Predictor map  
Mineral potential modelling  
Fuzzy inference systems  
Machine learning

## ABSTRACT

In this study we adopted fuzzy inference system (FIS), transformed predictor map-based random forest (RF) and feed-forward deep neural network (FF-DNN) approaches to mineral potential modelling (MPM) of the Granites-Tanami Orogen (GTO), Northern Territory, Australia, to (i) predict gold prospectivity, and (ii) compare the performance of these models to those previously generated in the study area. The current study, which utilized 19 predictor maps previously developed by Roshanravan et al. (2020) in the framework of a mineral systems approach, took into consideration the learnings gained and results obtained from previous approaches to modelling the gold potential of the GTO (Roshanravan et al., 2020: continuous fuzzy gamma, geometric average, data-driven index overlay and non-transformed predictor map-based RF; Roshanravan et al., 2021: cuckoo optimization algorithm). Importantly, our study area extending over > 46,000 km<sup>2</sup> in the GTO, represents one of the few, if not the only, areas worldwide that has been subjected to eight different modelling techniques, an approach that delivered unique insights that cannot be achieved by utilizing a single technique. For example, our multi-technique approach enabled us to study what effect predictor maps may have on model performance and resulting mineral potential maps. In the case of data-driven MPM with RF, arguably-one of the most popular machine learning techniques, the effect of non-transformed (i.e., original) and transformed (i.e., derivative) predictor maps has never been evaluated simultaneously. To achieve this, we generated a transformed predictor map-based RF potential model with the aim of comparing it to the non-transformed predictor map-based RF model of Roshanravan et al. (2020). The FF-DNN and Mamdani-type FIS approaches to MPM were carried out specifically for the purpose of comparing and further investigating the modelling results. With respect to the Mamdani-type FIS, the concentration-area (C-A) fractal technique served to more objectively determine thresholds of the underlying mathematical functions, a novel approach that aids in reducing bias resulting from human input and expert opinion. The thresholded results demonstrate that the RF potential map generated with transformed predictor maps outperformed all other data-driven and continuous models. Overall, our multi-technique approach to MPM and the comparing and contrasting of a large set of resulting gold potential models, not only offered insights that helped to develop and calibrate new tools and techniques but also delivered what we believe are more robust gold exploration targets. As a result, we strongly recommend to using a multi-technique approach to MPM, which we hope will soon replace the currently accepted and widely utilized single-technique approach.

\* Corresponding author at: Corporate Geoscience Group (CGSG), PO Box 5128, Rockingham Beach, WA 6969, Australia.

E-mail address: [opkreuzer@gmail.com](mailto:opkreuzer@gmail.com) (O.P. Kreuzer).

<https://doi.org/10.1016/j.oregeorev.2022.105224>

Received 21 August 2022; Received in revised form 20 November 2022; Accepted 21 November 2022

Available online 23 November 2022

0169-1368/© 2022 The Authors. Published by Elsevier B.V. This is an open access article under the CC BY license (<http://creativecommons.org/licenses/by/4.0/>).

## 1. Introduction

Non-renewable resources, such as mineral deposits, deplete as they are being exploited. To counteract mining depletion, new mineral resources, commonly concealed under younger sedimentary units, must be found and delineated. GIS-based mineral potential modelling (MPM) is being progressively utilized and accepted as an aid to reducing risk in mineral exploration targeting and a valuable addition to the 'exploration toolbox' (Hronsky and Kreuzer, 2019; Yousefi et al., 2019), offering a technology designed to improve the effectiveness of exploration targeting by (i) combining subjective human geological interpretation and objective machine-based analysis and (ii) capturing the best aspects of these complementary approaches (Bonham-Carter, 1994; Hronsky and Kreuzer, 2019; Kreuzer et al., 2020; Zuo et al., 2021; Behera and Panigrahi, 2022). However, more work is required by the modelling community with respect to more fully evaluating model input and its effect on model output so that one day a best-practice approach can be formulated.

In April 2020, the power of MPM as a targeting tool has been brought sharply into focus when Australian exploration company Chalice Mining Limited announced the discovery of Gonneville, a new tier-one palladium-platinum-nickel-cobalt-copper-gold deposit in Western Australia (Chalice Mining Limited, 2020). Gonneville is a greenfields discovery that was made on the back of a nickel-copper-platinum group metals prospectivity map generated by Geoscience Australia (Dulfer et al., 2016). The Gonneville discovery unlocked an entire new nickel-copper-platinum group metals search space along the > 1000 km-long, largely underexplored western margin of the Archean Yilgarn Craton of Western Australia (Australia's Mining Monthly, 2020). To our knowledge, the yet to be fully delineated Gonneville discovery (maiden resource of 330 Mt @ c. 0.58 % Ni eq. or c. 1.60 g/t Pd eq.: Chalice Mining Limited, 2021) represents the first world-class discovery that can, at least partly, be attributed to MPM and, thus, presents a proof-of-concept for this technology. Moreover, the MPM-assisted Gonneville discovery may mark a major game changer for this targeting tool in that it may result in greater acceptance and broader uptake of MPM by industry.

There are four common procedures used in MPM: (i) data-driven (or supervised), (ii) knowledge-driven, (iii) hybrid data- and knowledge-driven, and (iv) continuous approaches that operate on a set of

logistical functions (Carranza, 2008; Porwal and Kreuzer, 2010; Yousefi et al., 2019; Aryafar and Roshanravan, 2021). Typically, modelers only use one of these procedures in MPM of any given study area. However, applying multiple procedures is important as this is the only way that different methodologies can be benchmarked, compared and contrasted. One of the few exceptions is the Paleoproterozoic Granites-Tanami Orogen (GTO) of Australia's Northern Territory, which has been subjected to multiple MPM studies designed to predict areas of gold potential within this well-endowed but poorly exposed fold belt (Roshanravan et al., 2020, Roshanravan et al., 2021). The MPM completed by Roshanravan et al. (2020) (Fig. 1) utilized the data-driven RF and continuous geometric average, data-driven index overlay and fuzzy gamma techniques to compute gold prospectivity maps based on a set of 19 vetted (i.e., competent) predictor maps that capture the key ingredients of orogenic gold systems in the GTO and their mappable expressions. An evaluation of model performance revealed that the best performing gold potential map was generated by the RF method, which is known to diminish the problem of overtraining and enhance model performance (Breiman, 2001; Parsa and Maghsoudi, 2021). Subsequently, Roshanravan et al. (2021) applied their newly developed, data-driven cuckoo optimization algorithm to model the gold potential of the GTO, using the same study area, targeting model and input predictor maps as previously used and described by Roshanravan et al. (2020). The results of this study, in which the cuckoo optimization algorithm was combined with support vector regression (COA-SVR) and applied to transformed predictor maps (with proxy values in the range [0, 1]) derived from the original ones, showed that COA-SVR outperformed all prior MPM methods used by Roshanravan et al. (2020).

In this study, which is a follow-up to and expansion of previous research reported in Roshanravan et al. (2020, 2021), we added an additional set of modelling approaches to the existing MPM inventory pertaining to our study area in the GTO: i.e., (i) fuzzy inference system (FIS), (ii) transformed predictor maps-based RF and (iii) feed-forward deep neural network (FF-DNN) methods. Here we report the findings of this new study, chiefly designed to (i) develop a method for overcoming the exploration bias of FIS-driven MPM, which results from determination of mathematical function thresholds using expert opinion and consensus, and (ii) evaluate the effect of predictor maps on the performance of RF-driven MPM and resulting gold potential maps. With

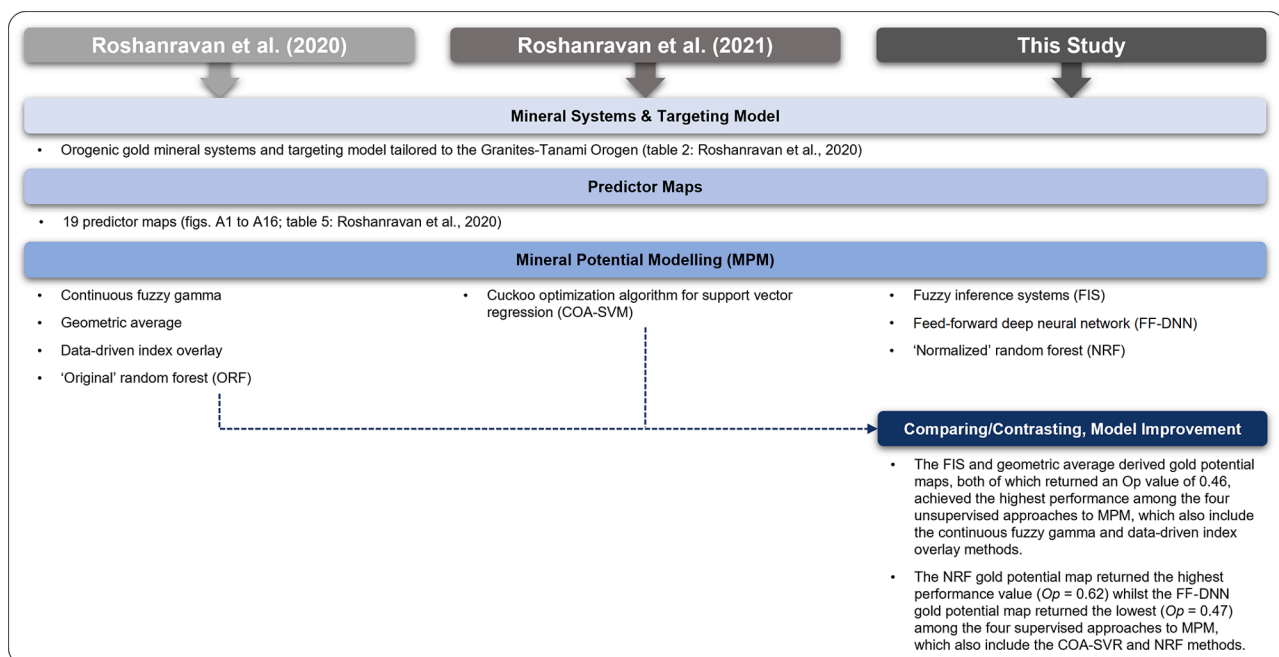
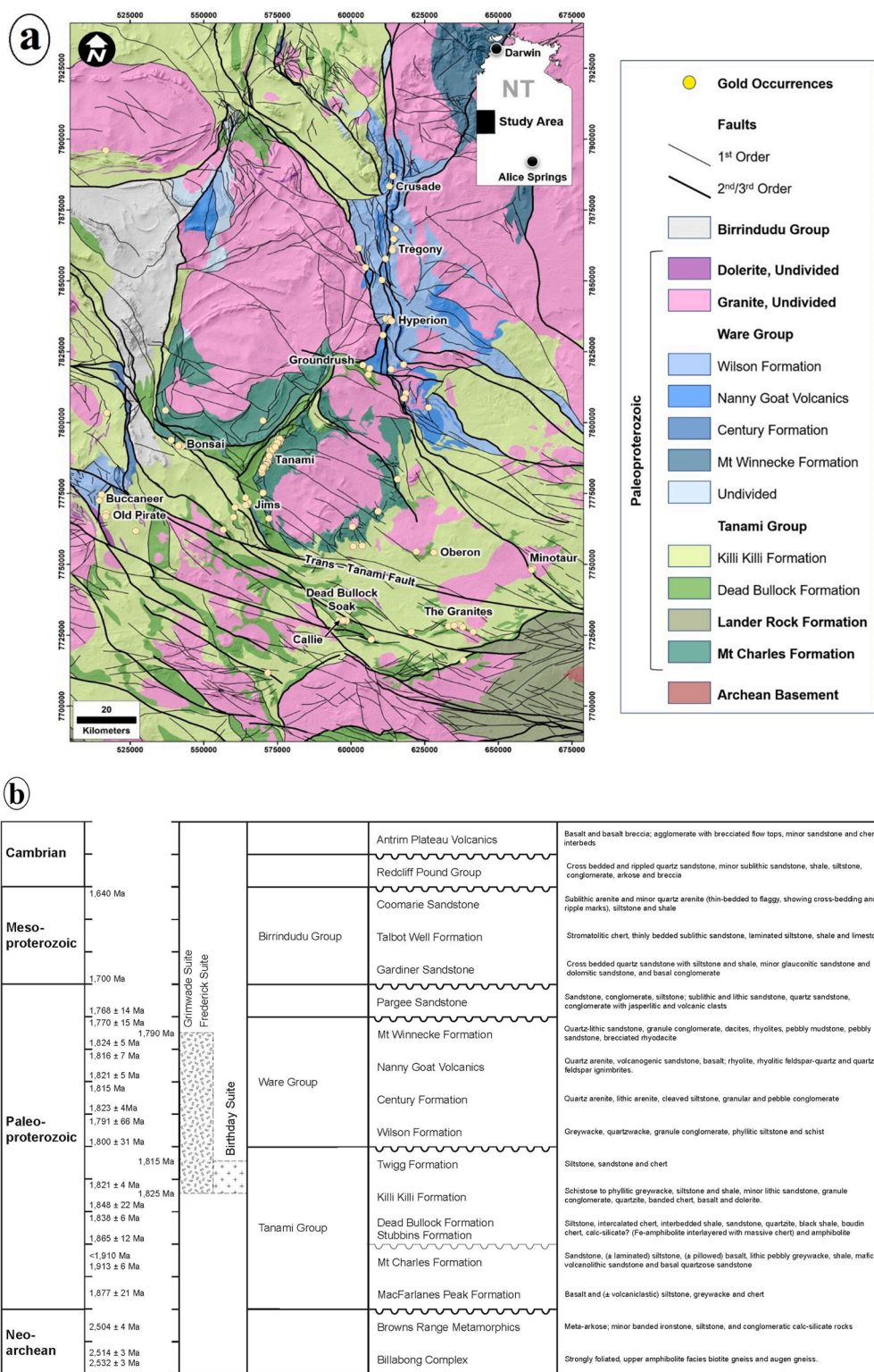
















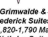
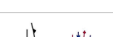
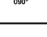
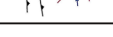
Fig. 1. Comparison of the 9 gold potential maps developed by Roshanravan et al. (2020, 2021, this study).



**Fig. 2.** (a) Solid geology map of the Granites-Tanami Orogen (GTO), Northern Territory (modified from Dr. Leon Vandenberg, unpublished data; reproduced from Roshanravan et al., 2020) also showing the main gold occurrences. Key gold camps and deposits are labelled. Inset map: Location of the study area in the western-central Northern Territory. The study area covers, wholly or partially, six 1:250,000 scale map sheets, namely Birrindudu (SE 5211), Winnecke Creek (SE 5212), Tanami (SE 5215), Tanami East (SE 5216), The Granites (SE 5203) and Mount Solitaire (SE 5204). (b) Lithostratigraphic framework for the GTO as published in Roshanravan et al. (2020), compiled from Crispe et al. (2007), Ahmad et al. (2013) and Bagas et al. (2008, 2010). (c) Schematic compilation of deformation events in the GTO as published in Roshanravan et al. (2020), compiled from Crispe et al. (2007), Bagas et al. (2010, 2014), Joly et al. (2010, 2012) and Ahmad et al. (2013). Key to abbreviations: DGTO = Deformation events pre- and syn-GTO as summarized in Bagas et al. (2010, 2014) and Joly et al. (2010, 2012); DPTO1-3 = Deformation events post-GTO as summarized in Bagas et al. (2010, 2014); Min = Mineralization events; Ign = Igneous events; Met = Metamorphic events; Tec = Tectonic setting.



**(c)**

	$\sigma_1$	Timing	Min	Mag	Structures	Comments
$D_{7+}$ $DPTO_3$						<b>Younger, post-1,790 Ma deformations</b> <ul style="list-style-type: none"> <li>Limited information</li> <li>Numerous late thrust faults, oblique slip faults and normal faults cutting earlier structures</li> </ul>
$D_6$ $DPTO_2$		ca. 1,790 Ma				<b>ENE-WSW- to E-W-directed shortening</b> <ul style="list-style-type: none"> <li>N-S- to NW-SE-striking D6 faults, including oblique thrusts with a component of left-lateral movement</li> </ul>
$D_5$ $DPTO_1$						<b>N-S- to NW-SE-directed shortening</b> <ul style="list-style-type: none"> <li>ENE-WSW- to E-W-trending, steeply SSE dipping angular F5 chevron folds</li> <li>S5 crenulations of earlier fabrics in F5 hinge regions and kink-bands</li> </ul>
$D_4$ $DGTO_3$		ca. 1,800 Ma				<b>NE-SW- to E-W-directed shortening</b> <ul style="list-style-type: none"> <li>Locally developed open, upright, angular NW-SE- to N-S-trending F4 folds</li> <li>Local S4 crenulation of S2 fabric in F4 hinge regions</li> <li>Rare oblique F2- and F4-fold interference structures</li> <li>D4 was associated with greenschist facies metamorphism</li> </ul>
$D_3$ $DGTO_2$						<b>NW-SE- to WNW-ESE-directed shortening</b> <ul style="list-style-type: none"> <li>Asymmetrical and angular NE-SW- to NNE-SSW-trending F3 folds of ca. 1 km wavelength</li> <li>Local planar S3 fabric crenulating pre-existing S2 fabric in F3 hinge regions</li> <li>Tight to isoclinal refolding of D2 structures by F3 folds</li> <li>D3 was associated with greenschist facies metamorphism</li> </ul>
$D_2$ $DGTO_1$		ca. 1,850 Ma				<b>E-W-directed shortening</b> <ul style="list-style-type: none"> <li>Disharmonic, tight to isoclinal, moderately- to steeply-plunging, N-S- to NNNW-SSE-, WNW-ESE- and NE-SW-trending F2bids modified/refolded by later deformations</li> <li>Well-developed axial planar S2 cleavage and L2 stretching lineations in F2 hinge regions and parallel to F2</li> <li>Thrusts and transpressional faults mainly parallel to S2</li> <li>D2 represents an oblique inversion of the D1 architecture and is interpreted as a thin-skinned tectonic event</li> <li>D2 was associated with greenschist to middle amphibolite facies metamorphism</li> </ul>
$D_1$ $DGTO_0$		ca. 1,865 Ma				<b>N-S- to NNE-SSW-directed extension</b> <ul style="list-style-type: none"> <li>WNW-ESE-striking, S-dipping, listric, crustal-scale faults, including orogen-parallel normal faults and orogen-transverse transfer faults, produced during an early rifting event</li> <li>The rift architecture appears to have played a fundamental role in controlling the location of later D2 structures</li> <li>Amphibolite-facies metamorphism of the Neoproterozoic Billabong Complex predates deposition of the Tanami Group</li> </ul>

**Tanami Orogeny**

Fig. 2. (continued).

respect to the latter, we also perused the effect of using original, non-transformed versus derivative, transformed predictor maps with proxy values in the range [0, 1]. As argued in this paper, such investigations, which have never been conducted in MPM, can aid in reducing uncertainty and generating more reliable exploration targets.

## 2. Geology and gold mineralization of the Granites-Tanami Orogen (GTO)

### 2.1. Geological background

The GTO (Fig. 2a), a remote, largely concealed and poorly understood fold belt straddling the border between the Northern Territory and Western Australia, preserves a complex record of Paleoproterozoic basin development, deformation and magmatism along the southern margin of the North Australian Craton. Extensive Neoproterozoic to Phanerozoic sedimentary cover conceals its contacts with other Palaeoproterozoic fold belts of the North Australian Craton such as the Halls Creek Orogen to the northwest, Arunta Orogen to the southeast and Tennant Creek Orogen to the east (Cawood and Korsch, 2008; Bagas, 2010; Bagas et al., 2014; Ahmad et al., 2013; Maidment et al., 2020).

The oldest units in the GTO are Neoproterozoic metaigneous and metasedimentary basement rocks of the Browns Range Metamorphics (ca. 2530 to 2500 Ma) and Billabong Complex (ca. 2514 Ma) that occur as isolated inliers within Paleoproterozoic (ca. 1,877 to 1,838 Ma), mostly greenschist facies metamorphic grade sedimentary and volcanic rocks of the Tanami Group (Crispe et al., 2007; Ahmad et al., 2013; Bagas et al., 2008, 2010; Maidment et al., 2020) (Fig. 2a, b). The latter is unconformably overlain by siliciclastic sedimentary and felsic volcanic rocks of the Ware Group, which were deposited between ca. 1825 and 1810 Ma, postdating regional deformation and greenschist to amphibolite facies metamorphism during the ca. 1830 Ma event of the prolonged Tanami Orogeny (Fig. 2c).

Voluminous granitic intrusions of the Birthday, Grimwade, and Frederick suites, typically comprised of peraluminous, calcic to calc-alkalic, I-type granodiorite to monzogranite, intruded between ca. 1825 and 1790 Ma (Cawood and Korsch, 2008; Bagas, 2010; Bagas et al.,

2014; Ahmad et al., 2013; Maidment et al., 2020), following peak metamorphism and deformation during the ca. 1850–1840 Ma event of the Tanami Orogeny (Li et al., 2014) (Fig. 2c).

Late Palaeoproterozoic (<1768 Ma) conglomerate, sandstone and siltstone of the Pargee Sandstone, interpreted to have been deposited in a restricted molasse-type basin, and Mesoproterozoic (ca. 1735–1640 Ma) sandstone, shale and limestone of the Birrindudu Group, interpreted to have been deposited in a shallow-marine shelf setting, postdate both granite emplacement and the Tanami Orogeny (Fig. 2c) and unconformably overlie the older successions (Crispe et al., 2007).

### 2.2. Tectonic setting and evolution

Consensus is emerging with respect to the Palaeoproterozoic Tanami Group having been deposited in a back-arc environment above a north-dipping subduction zone at ca. 1865 Ma. Basin inversion during the Tanami Orogeny between ca. 1850 and 1800 Ma (Fig. 2c) was linked to and driven by rapid accretion of several micro-continents along the margin of the proto-North Australian Craton during the assembly of the Nuna supercontinent (Bagas et al., 2010, 2014; Joly et al., 2010, 2012; Betts et al., 2016).

### 2.3. Gold mineralization

The GTO is host to a significant gold endowment totaling over 20 Moz Au. Most of this endowment is captured in the Dead Bullock Soak (>12.0 Moz Au), Tanami (2.0 Moz) and Granites (>1.0 Moz Au) gold deposit clusters as well as a handful of important deposits such as Titania-Oberon (>5.0 Moz Au), Groundrush (1.5 Moz Au), Buccaneer (0.6 Moz Au) and Coyote-Bald Hill (0.5 Moz Au) (Wygralak et al., 2005; Huston et al., 2007; Baggott et al., 2016; Roshanravan et al., 2020).

Gold mineralization, which is commonly classified as orogenic type, was associated with collisional tectonics, in particular late-stage compression and coeval magmatism at c. 1800 to 1790 Ma (Bagas et al., 2014; Maidment et al., 2020; Joly et al., 2012; Roshanravan et al., 2020), and postdates peak metamorphism (1839 ± 9 Ma: Petrella et al., 2020) by several tens of millions of years.



**Table 1**

Critical processes and spatial proxies for orogenic gold deposits in the study area (Roshanravan et al., 2020).

Critical Processes	Predictor Maps	Rationale
Transport	Domains of greater metallogenic trend line density	There is a strong spatial association between the known gold deposits and metallogenic trends, defined as directions of maximum continuity of gold deposit alignment as revealed by a Fry analysis. These trends are thought to be representative of basement structures acting as first-order controls on fluid flow.
	Proximity to D1 and D2 folds	Folds (i.e., anticlines and synclines) are known to host gold mineralization and while synclines may be less well-endowed, they are often less explored.
	Domains of greater metallogenic trend line intersection density	As outlined above, these trends are thought to be representative of basement structures acting as first-order controls on fluid flow. Fluid flow would likely have been enhanced at the intersection of permeable basement structures.
	Domains of greater fault density	Greater fault density is assumed to be associated with a greater likelihood of dilation, brecciation and fluid flow.
	Proximity to domains of remanent magnetisation	The remanent magnetization can be interpreted as a proxy for gold-related hydrothermal fluid flow and the structures that controlled the location of gold mineralization.
	Proximity to faults	The second- and third-order faults possibly represent major camp- to district-scale fluid pathways.
	Proximity to major faults	The major, first-order faults act as fundamental, first-order controls on hydrothermal fluid migration in the upper crust at the time of gold deposition.
	Proximity to gravity worms	The gravity worms with the highest levels of upward continuation can be interpreted as long-lived, multiply reactivated, deep-seated basement structures that would have acted as first-order controls on fluid migration.
	Proximity to gravity lineaments	The gravity data respond well to the deeper crustal architecture in the basement to the GTO and provide clues as to where these deep-seated structures may have interacted with those of the upper crust (i.e., the “thin-skinned” tectonic domain) to control the location of gold mineralization.
	Proximity to pseudogravity worms	The pseudogravity worms with the highest levels of upward continuation can be interpreted as upper-crustal faults and shear zones and, thus, potential fluid pathways.
Trap	Proximity to compositionally heterogeneous rock packages	These units are interpreted to be more likely to develop breaching or damage zones that may give rise to localized fracturing, dilation and permeability, focusing fluid flow at or close to lithological contacts and/or to possess strong chemical gradients across internal lithological boundaries that may

**Table 1 (continued)**

Critical Processes	Predictor Maps	Rationale
Deposition	Proximity to fault/fold intersections	give rise to redox reactions and destabilization of gold complexes carried by hydrothermal fluids. Fault/fold intersections encompasses the intersections between faults and pre-D3 folds. These intersections represent potential highly favorable trap sites.
	Domains of greater fault intersections density	Greater fault intersections density represents potential breaching/damage zones, which may have acted to enhance fluid flow and as physical traps.
	Domains of greater lithological contact density	Domains of greater lithological contact density are considered to have enhanced potential for rheological and chemical contrast.
	Proximity to contacts between the Dead Bullock and Killi Killi formations	These contacts separate stratigraphic units of potentially high rheological $\pm$ chemical contrast.
	Proximity to potential host lithologies	All pre-Mesoproterozoic lithologies in the GTO have potential for hosting gold deposits and collectively constitute the gold permissive tract.
	Proximity to geochemical anomalies	Known gold deposits in the GTO have gold and pathfinder element (As, Ag, Bi, Cu, Mo and Sb) geochemical signatures. Anomalous Au, As, Ag, Bi, Cu, Mo and Sb values were extracted from a large, proprietary, GTO-wide geochemical database comprising > 164,000 surface and > 93,000 interface (mostly vacuum and rotary air blast drilling) samples.
	Domains of greater quartz vein density	Domains of greater quartz vein density acts as a proxy for structural permeability and hydrothermal activity.
	Domains of greater mafic dyke density	Areas of greater density of mafic dykes are considered to have elevated potential for lithological competency gradients and geochemical gradients.
	Readers are referred to Roshanravan et al. (2020) for original rationales and definitions.	

A comprehensive summary of the main gold deposits in the GTO, including discovery years, contained resources, host rocks, deformation histories, host structures and ore controls, deposit dimensions and orientations, mineralization and ore styles, ore and gangue mineralogies, ore element associations, vein parageneses, alteration types and assemblages, ore fluid characteristics, ‘exploration vectors’, mineralization ages, metamorphic grades and genetic models, is provided in Roshanravan et al. (2020).

### 3. Mineral potential modelling (MPM) and input predictor maps

Generating appropriate, well-performing predictor maps and choosing robust, fit-for-purpose modelling tools are key ingredients for success in MPM. As discussed by Hronsky and Kreuzer (2019), it is common that the input data do not uniformly and objectively represent the search space of interest, omit critical targeting-relevant parameters and have a large degree of unrecognized dependence.

The construction of robust predictor maps requires an in-depth comprehension of the key ore-forming processes of the targeted ore

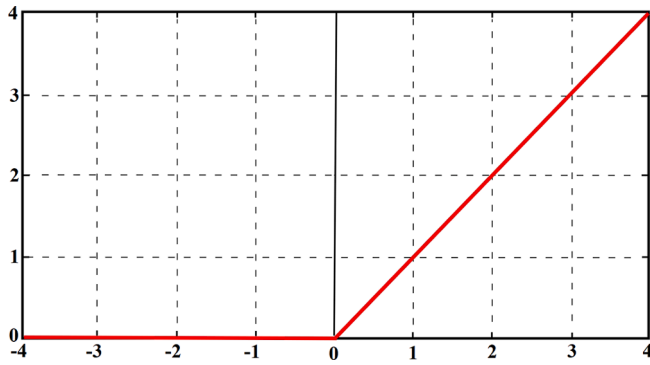


Fig. 3. Diagram of the ReLU activation function.

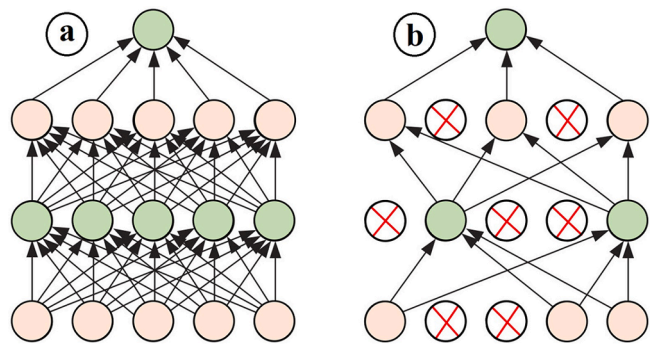


Fig. 4. The Dropout neural net model: (a) a standard neural net and (b) an example of a thinned net generated by exerting dropout (Modified from Srivastava et al., 2014).

deposit type and their mappable expressions (also known as spatial proxies). This, in turn, necessitates a holistic ore deposit and exploration targeting model. We believe that these types of models are best developed in the framework of a mineral systems approach (e.g., Wyborn et al., 1994; Kreuzer et al., 2008; McCuaig et al., 2010; Tessema, 2017; Roshanravan, 2020; Maepa et al., 2021). As summarized by Kreuzer et al. (2019), the minerals system concept is far more flexible and much broader in its reach than the traditional, forensic and deposit-centric source–transport–trap analysis in that it considers ore deposit formation in the framework of much larger lithospheric-scale processes.

We also strongly advocate a ‘multi-technique approach’ to MPM; that is the generation and integrated use of multiple mineral prospectivity models of the same targeting area produced by different MPM tools (e.g., Joly et al., 2012; Chudasama et al., 2018; Roshanravan et al., 2020). This is a relatively new and, as of yet, underutilized approach but one that (i) ensures optimization of the available conceptual and empirical information, (ii) helps to better understand and minimize stochastic and systemic uncertainties, (iii) facilitates cross-validation of the resulting prospectivity models, and (iv) allows the resulting models to be compared and contrasted.

In this study, we employed 19 robust, vetted (i.e., competent) predictor maps that were developed in the framework of a mineral systems approach (Roshanravan et al., 2020) (Table 1). These predictor maps represent spatial proxies of the key mappable processes of orogenic gold

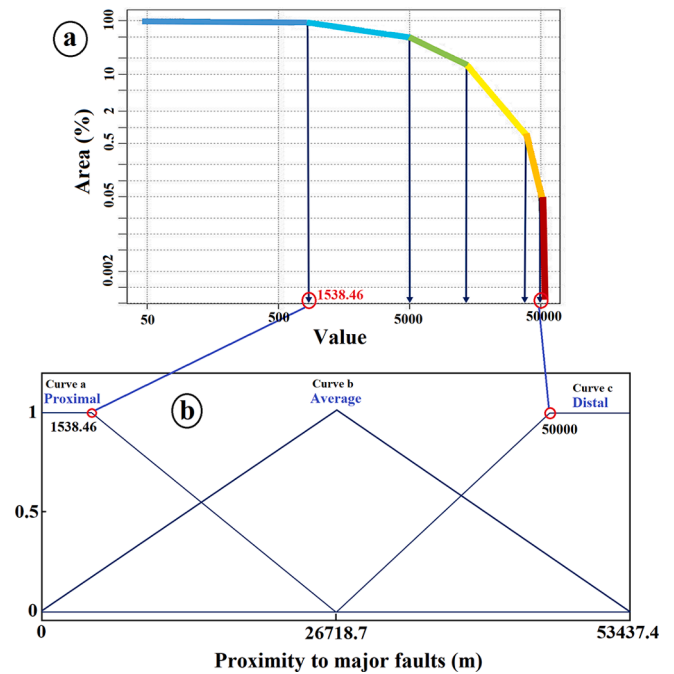


Fig. 6. Transport — (a) Concentration-area fractal plot for proximity to major faults and (b) piece-wise linear membership function plot for proximity to major faults.

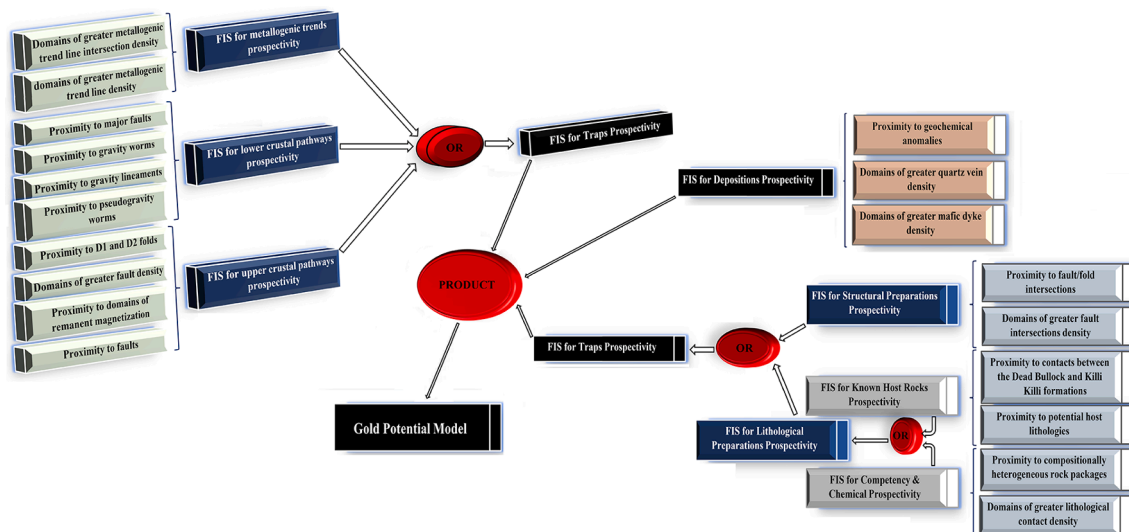


Fig. 5. FIS-based potential modelling flow chart.

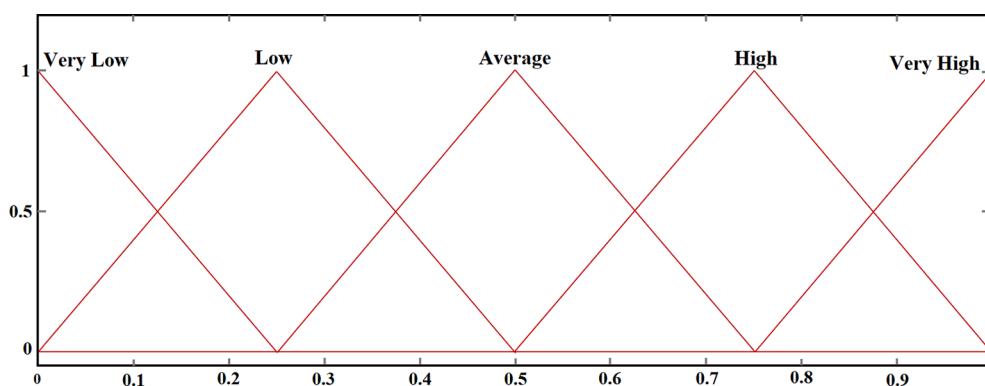


Fig. 7. Piece-wise linear membership function plot for gold potential.

**Table 2**  
Input variables and linguistic values.

Critical processes	Input variables (predictor maps)	Linguistic values
Transport	Metallogenic Trend Proxies	
	1. Domains of greater metallogenic trend line intersection density	Low, Average, High
	2. Domains of greater metallogenic trend line density	Low, Average, High
	Lower Crustal Pathway Proxies	
	3. Proximity to major faults	Proximal, Average, Distal
	4. Proximity to gravity worms	Proximal, Average, Distal
	5. Proximity to gravity lineaments	Proximal, Average, Distal
	6. Proximity to pseudogravity worms	Proximal, Average, Distal
	Upper Crustal Pathway Proxies	
	7. Proximity to D1 and D2 folds	Proximal, Average, Distal
Trap	8. Domains of greater fault density	Low, Average, High
	9. Proximity to domains of remanent magnetization	Proximal, Average, Distal
	10. Proximity to faults	Proximal, Average, Distal
	Structural Preparation Proxies	
	11. Proximity to fault/fold intersections	Proximal, Average, Distal
	12. Domains of greater fault intersections density	Low, Average, High
	Lithological Preparation Proxies	
	A. Known Host Rock Proxies	
	13. Proximity to contacts between the Dead Bullock and Killi Killi formations	Proximal, Average, Distal
	14. Proximity to potential host lithologies	Proximal, Average, Distal
Deposition	B. Competency & Chemical Contrast Proxies	
	15. Proximity to compositionally heterogeneous rock packages	Proximal, Average, Distal
	16. Domains of greater lithological contact density	Low, Average, High
	Deposition Proxies	
	17. Proximity to geochemical anomalies	Proximal, Average, Distal
	18. Domains of greater quartz vein density	Low, Average, High
	19. Domains of greater mafic dyke density	Low, Average, High
	Consequent variables	
	Gold Potential	Very low, Low, Average, High, Very high

mineralization as pertaining to the GTO.

### 3.1. Methodology

#### 3.1.1. Fuzzy inference systems (FIS)

Fuzzy inference systems (FIS) are based on the theory of fuzzy sets (Zadeh, 1973) in that they are composed of a series of if-then rules expressed in natural language representing expert reasoning. In the context of MPM (Porwal et al., 2015), this reasoning relates to the prediction of mineral prospectivity based on the syntax of linguistic predictor variables. In an if-then rule, the membership of linguistic values for the related predictor maps is computed through a predefined membership function. A number of fuzzy if-then rules are then compiled to create an FIS. These fuzzy if-then rules use linguistic terms (e.g., low/moderate/high) for various syntax of the linguistic values of the input predictor maps to predict the mineral prospectivity (Porwal et al., 2015). To generate the FIS output, a suitable aggregation method is used to synthesize the outputs of individual rules, and then the aggregate area is turned into a single output through a defuzzification procedure. The final output, therefore, is a single value between 0 and 1 that represents the mineral potential score. It is important to note, however, that the FIS technique carries bias because the relevant 'if-then' fuzzy rules and thresholds of the mathematical functions require expert input and opinion. To reduce this handicap, here we employed the concentration-area (C-A: Cheng et al., 1994) fractal technique designed to objectively determine the thresholds of the mathematical functions.

The following stages are required in the execution of an FIS (Porwal et al., 2015):

- Produce a conceptual/descriptive model for the targeted mineral systems and determine the exploration/targeting criteria. Generate suitable predictor maps (or spatial proxies) for the targeting criteria by processing geo-datasets with GIS and programming tools. The FIS uses predictor maps as input variables, and the output variables are mineral-system-components potential, including energy source potential, trap potential, transport potential and deposition potential.
- Designate the linguistic values for each predictor map. For instance, anticline is a proxy that hosts gold mineralization in orogenic gold systems. The conceivable linguistic values for anticline can be {very proximal, proximal, intermediate, distal, very distal}. A similar process should be utilized to determine the linguistic values for each of the output mineral-system-component potential ('low transport potential', 'high deposition potential', etc.).
- Translate the categorical or numerical values of each input predictor map into fuzzy scores using an appropriate membership function.
- Create an FIS for each individual component of the mineral system, including chemical and physical traps, deposition, transport and energy source. The reasoning of an exploration expert should be captured by the FIS, and as a result, the FIS should capture all



## Metallogenic Trends

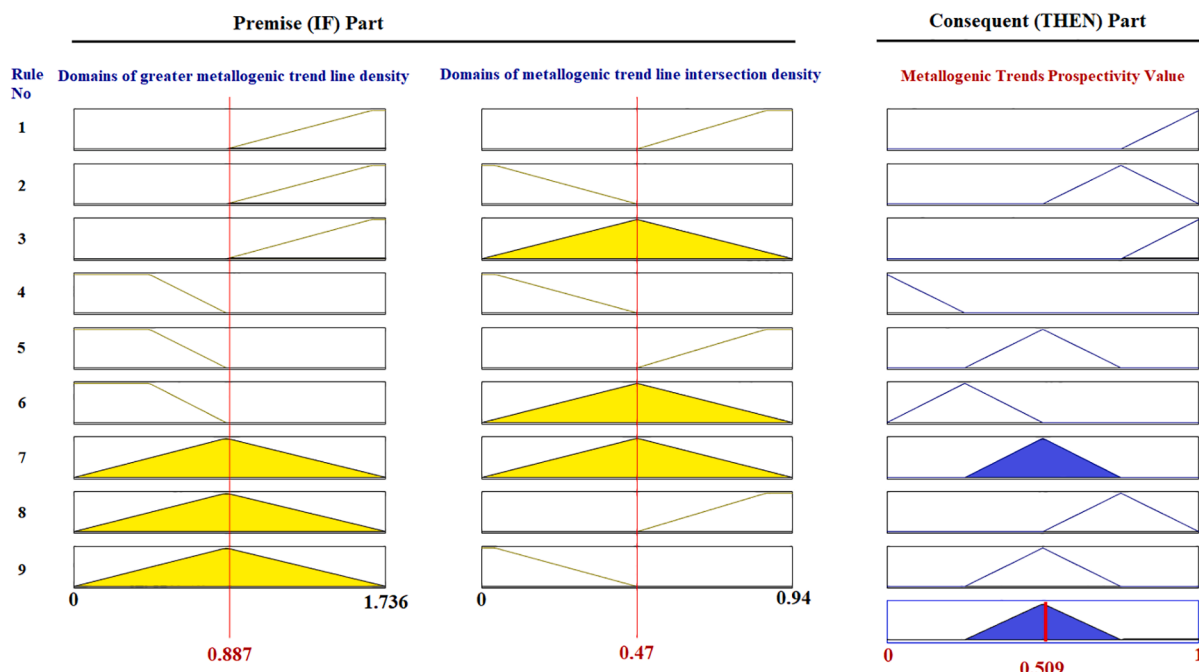


**Fig. 8.** Metallogenic trend FIS rules: the fuzzy inference systems applied for potential modelling of gold deposits in the GTO. An example for a cell with values [0.887, 0.47] on the two spatial proxies for metallogenic trend: (1) domains of greater metallogenic trend line density, (2) domains of greater metallogenic trend line intersection density, respectively, is illustrated. The values are marked by red lines. The values of activated fuzzy membership are shown in yellow (if the activated fuzzy membership value for a certain input value is 0, the fuzzy functions are blank). In the consequent part, having truncated an output consequent function by the firing strength of the rule, the remaining area of that function have been shown by the blue part. The last function of the output potential column represents the aggregate of all output fuzzy functions. The defuzzified crisp value (0.509) that represents the occurrence feasibility of metallogenic trends in the certain cell has been shown by the red line. (For interpretation of the references to colour in this figure legend, the reader is referred to the web version of this article.)

**Table 3**

Metallogenic trends FIS rules.

Premise (IF) part				Consequent (THEN) part	
1. IF	Metallogenic trend line density is high	AND	Domains of metallogenic trend line intersection density is high	Then	Metallogenic trend prospectivity is very high
2. IF	Metallogenic trend line density is high	AND	Domains of metallogenic trend line intersection density is low	Then	Metallogenic trend prospectivity is high
3. IF	Metallogenic trend line density is high	AND	Domains of metallogenic trend line intersection density is average	Then	Metallogenic trend prospectivity is very high
4. IF	Metallogenic trend line density is low	AND	Domains of metallogenic trend line intersection density is low	Then	Metallogenic trend prospectivity is very low
5. IF	Metallogenic trend line density is low	AND	Domains of metallogenic trend line intersection density is high	Then	Metallogenic trend prospectivity is average
6. IF	Metallogenic trend line density is low	AND	Domains of metallogenic trend line intersection density is average	Then	Metallogenic trend prospectivity is low
7. IF	Metallogenic trend line density is average	AND	Domains of metallogenic trend line intersection density is average	Then	Metallogenic trend prospectivity is average
8. IF	Metallogenic trend line density is average	AND	Domains of metallogenic trend line intersection density is high	Then	Metallogenic trend prospectivity is high
9. IF	Metallogenic trend line density is average	AND	Domains of metallogenic trend line intersection density is low	Then	Metallogenic trend prospectivity is average

pragmatically feasible syntaxes of the proxies' linguistic values. A precise deliberation of the geological connections between two input predictor maps, including conditional associations between the two with regard to the targeted mineral systems, is required before selecting the coordinate operator (disjunction or conjunction) between the two input predictor maps.

- Compute the strength of each rule's firing. The strength of a rule's firing is the cumulative fuzzy membership value of the rule's if-part. Fuzzy disjunction or fuzzy conjunction can be utilized to compute the fuzzy membership scores for the input predictor maps in the if-part. Fuzzy Algebraic Sum ( $= 1 - \prod_i^n (1 - \mu_i)$ , where  $n$  is the number of input variables and  $\mu$  is the fuzzy membership score) and OR are fuzzy disjunction (s-norm or t-conorm) operators that generalize

union and return, respectively, the sum and maximum of the input fuzzy membership scores. Alternatively, Fuzzy Algebraic Product ( $= \prod_i^n \mu_i$ , where  $n$  is the number of input variables and  $\mu$  is the fuzzy membership score) and AND are t-norm/conjunction operators that implement generalized intersection and return, respectively, the product and minimum of the input fuzzy membership scores.

- The strength of each fuzzy if-then rule's firing is utilized to scale down the rule's fuzzy output. Scaling down the output can be accomplished by different methods such as Max-Product or Min-Max. The latter method truncates the output fuzzy set determined via the then-membership function to the firing strength level. The former method scales down the then-membership function in symmetry to the firing strength through multiplying it by the firing

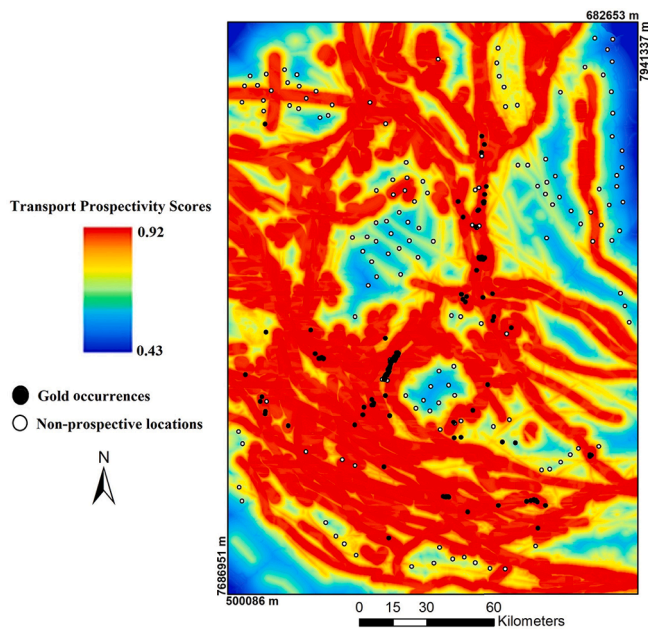


Fig. 9. Transport prospectivity map.

strength. Instead of a single point representing a fuzzy membership score, the output in both cases is an area under curve representing a fuzzy set.

- The areas-under-curve generated by individual rules are aggregated to define the ultimate output of an FIS. The MAX procedure is the most generally utilized methods that its output is the union of all areas. A defuzzification technique is finally utilized to turn the aggregate area into a point value. The centroid technique is one of

the most extensively utilized defuzzification methods that involves finding the aggregated area's gravity center. An FIS's output point value renders a given mineral systems component's potential.

- Mineral systems approach assumes that a deposit can only form if all incumbent processes are present, hence using a conjunction operator like AND or Algebraic Product, the output prospectivity can be computed as follows:

Prospectivity = MIN(Transport potential, Trap potential, Deposition potential),

or

Prospectivity = Transport potential  $\times$  Trap potential  
 $\times$  Deposition potential.

It is conceivable to theoretically develop a complicated FIS that can output the targeted deposit's potential, and therefore can be applied for quantitatively estimating resources. Such estimations, however, can be trustworthy only if the geo-datasets are meticulous and the targeted mineral systems are precisely modeled.

### 3.1.2. DecimalComplex, 3.1.2., DecimalComplex, 3. Random forest (RF) algorithm

Despite the fact that a wide variety of supervised machine learning algorithms have been utilized for MPM (e.g., Zhang et al., 2021; Maepa et al., 2021; Parsa, 2021; Roshanravan et al., 2021; Yang et al., 2022), many studies have lately demonstrated the effectiveness of RF-driven MPM (Carranza and Laborte, 2015; Ford, 2020; Wang et al., 2020; Xiang et al., 2020; Daviran et al., 2021; Zhang et al., 2021) and the superiority of it over other machine learning algorithms applied for MPM (Rodriguez-Galiano et al., 2015; Roshanravan, 2020; Keykhay-Hosseinpour et al., 2020). This is because the RF technique diminishes the problem of over-training and enhances the performance of models using a bagging procedure (Breiman, 2001; Parsa and Maghsoudi, 2021).

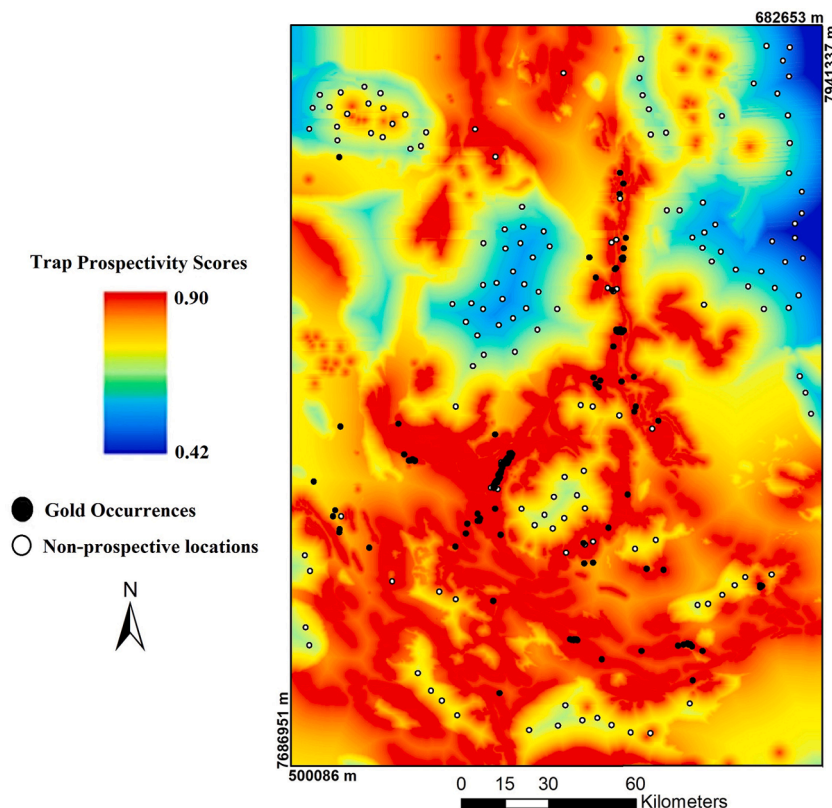


Fig. 10. Trap prospectivity map.

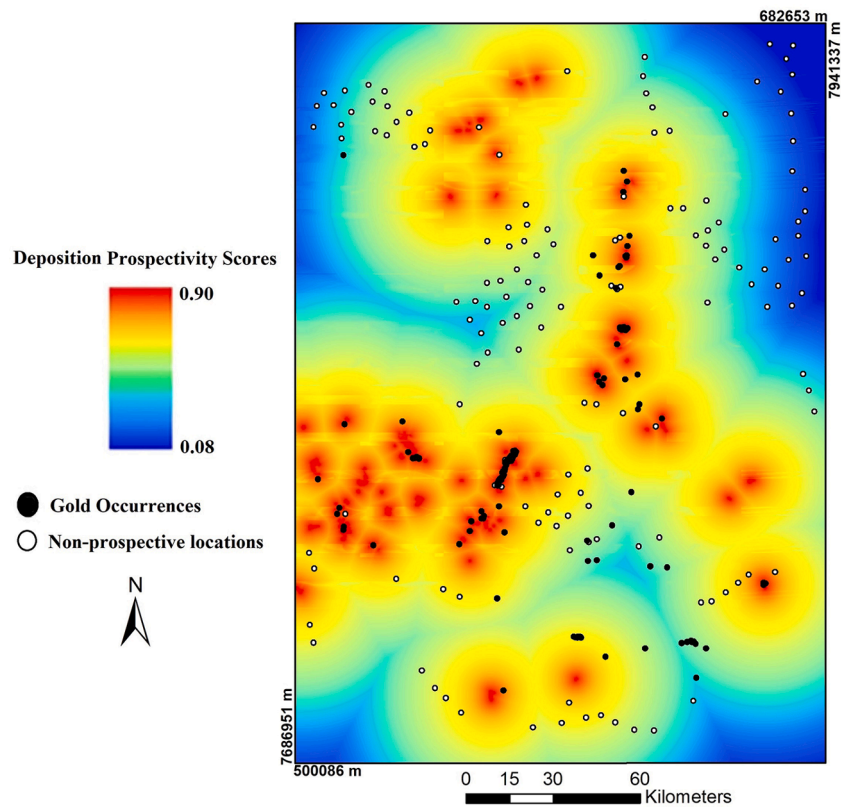


Fig. 11. Deposition prospectivity map.

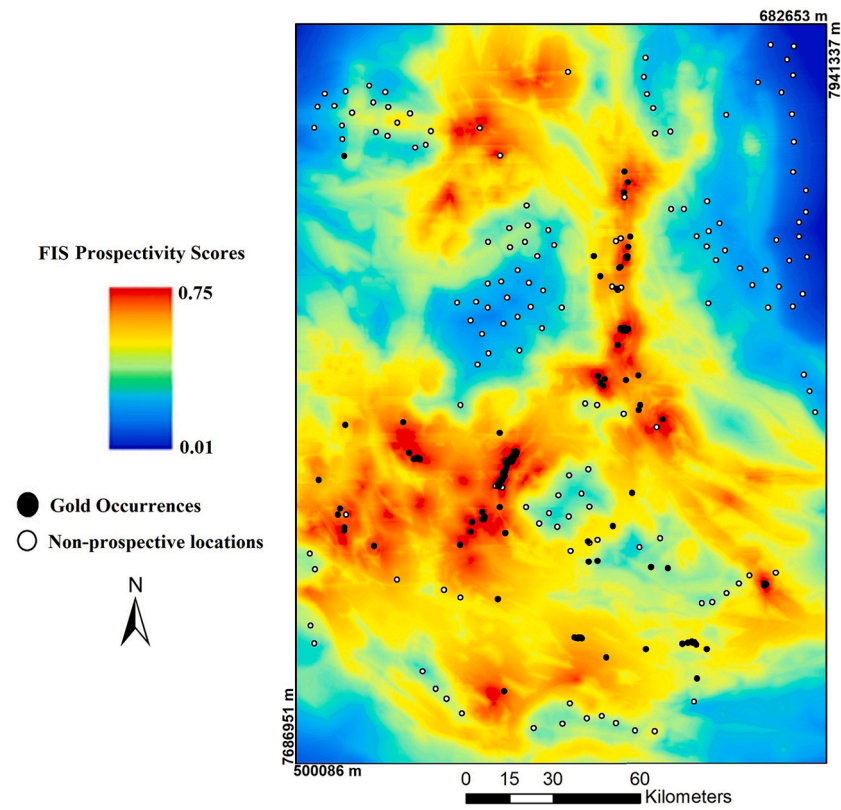


Fig. 12. Orogenic gold potential map generated by the FIS technique.



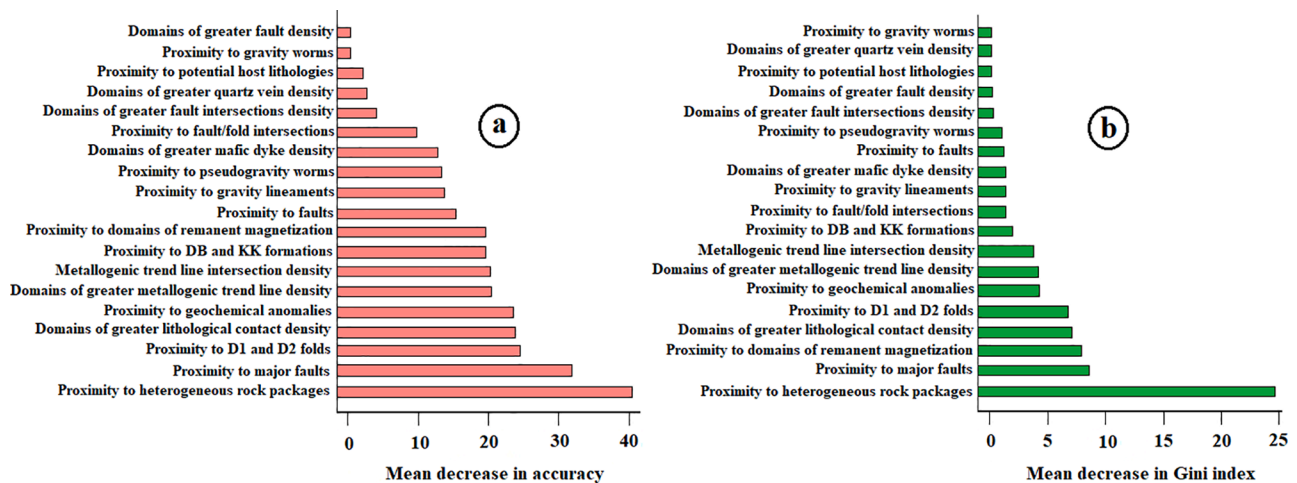


Fig. 13. Measure of predictor variable importance derived by RF technique: (a) mean decrease in accuracy and (b) mean decrease in Gini impurity index.

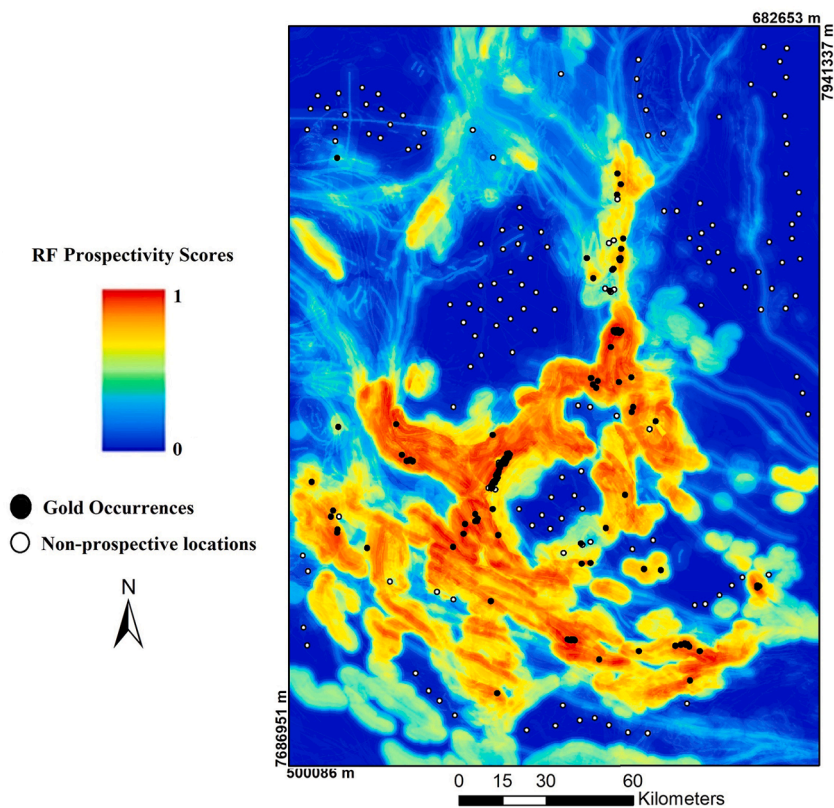


Fig. 14. RF potential map generated by combining the 19 normalized competent predictor maps.

The tools of ensemble learning have been utilized to enhance the performance of machine learning techniques (Dietterich, 2002; Parsa, 2021). Random forest (RF) (Breiman, 2001) is an ensemble-based machine learning algorithm that employs a resampling technique for generating each random set of training samples applied to develop an unpruned decision tree (cf. Breiman, 2001). In this regard, a bootstrapping approach that takes sub-samples with replacement from the values of predictor maps at prospect and non-prospect locations, termed labeled data, is utilized as the resampling technique. As such, two-thirds of the labeled data, termed in-bag samples, are utilized for training decision trees, while the remainder, termed out-of-bag (OOB) samples, are utilized to measure the OOB error, termed decision tree impurity. Hence, RF is an aggregation of unpruned decision trees, each of which is

constructed pursuant to a various set of extant patterns.

Running RF requires two parameters: (i) the number of predictor variable ( $m$ ) to be entered at each node, and (ii) the number of trees ( $n$ ) to be grown (Breiman, 2001). These parameters should be optimized so that the OOB error is minimized. The mean decrease in the accuracy ( $M_a$ ) and Gini impurity index ( $M_G$ ) can be utilized to measure the significance of predictor variables. The former is determined by the calculation of the OOB error, while the latter is a measure of how each variable contributes to the homogeneity of the nodes and the ultimate RF model (Breiman, 2001). Pursuant to Breiman (2001), the higher the values of Gini index and LSE, the more important predictor. Readers are referred to Breiman (2001) for further information on RF.

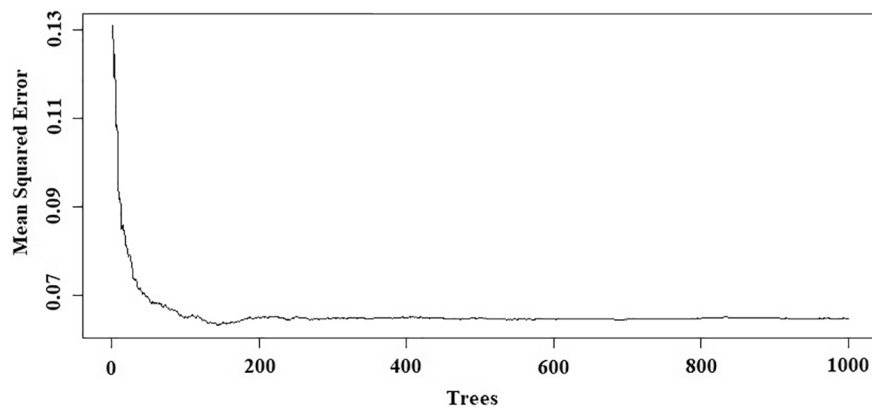


Fig. 15. Evolution of mean squared error curve for exploration evidential data used for training the RF potential model.

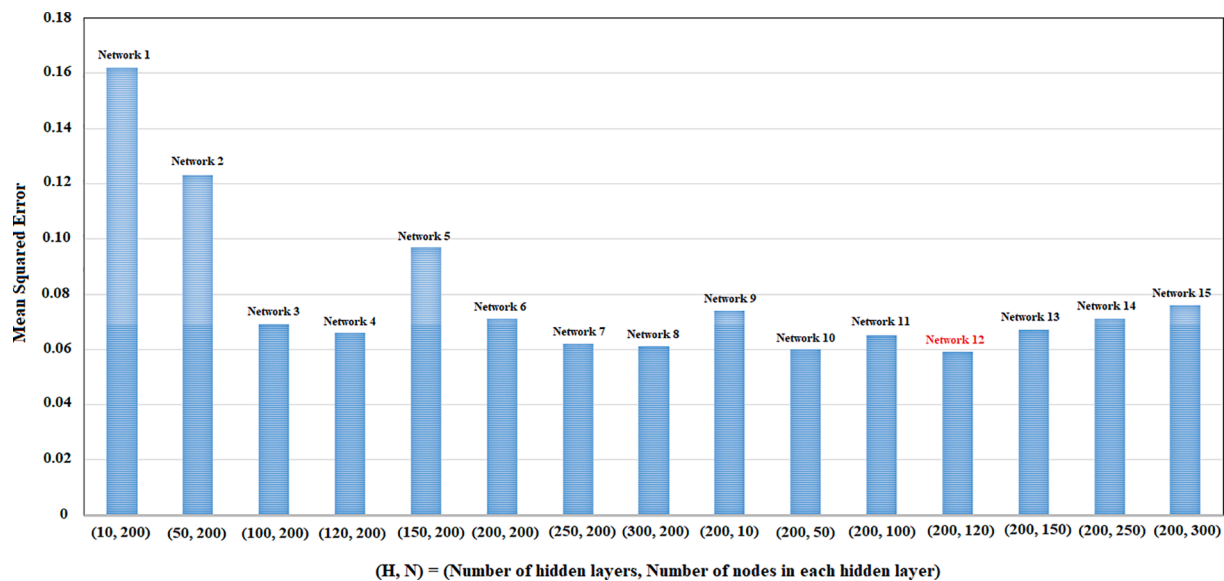


Fig. 16. Mean squared error for different networks.

#### 4. 1.3.,DecimalComplex,3.1.3.,DecimalComplex,3. Feed-forward deep neural network

In recent years, deep learning methods have been increasingly used to aid problem solving in the earth sciences. Deep learning methods are typically classified as unsupervised and supervised algorithms both of which have been effectively employed in MPM (Sun et al., 2020; Xiong et al., 2018; Xu et al., 2021; Zhang et al., 2021; Parsa et al., 2022). Feed-forward deep neural network (e.g., Xu et al., 2021), convolutional neural networks (e.g., Sun et al., 2020; Zhang et al., 2021), deep autoencoder network (Xiong et al., 2018) and the group method of data handling (GMDH) neural networks (e.g., Parsa et al., 2022) are among the more popular methods currently used in MPM.

Deep learning methods, in which the term “deep” refers to the number of layers through which the data are transformed, are representation-learning methods based on artificial neural networks (ANNs: Bengio, 2009; LeCun et al., 2015). Deep learning methods, unlike the shallow machine learning methods that generally do not learn progressive representations, render multiple levels of representation acquired by forming simple but non-linear modules. Each level learns to transform its input data into a representation at a slightly more abstract level. Accordingly, very complicated functions can be learned by composition of enough such transformations (Bengio, 2009; LeCun et al., 2015). The role of deep learning architecture is learning complex

functions indicating higher level representations. Feed-forward neural network architectures that process data in multi-layers and elicit all optimal parameters in the training process are utilized in many deep learning applications (Glorot and Bengio, 2010; Goodfellow et al., 2016). In this study, a feed-forward neural network was utilized as the regression neural network for MPM of gold deposits in the GTO.

Neurons that serve as the principal units forming neural networks are made up of several parts: an input, parameters, activation functions, and outputs (Zhou, 2016). Each neuron, termed a node, will have parameters (weights and biases) to train per each node from the preceding layer. In this study, the back propagation (BP) algorithm (e.g., Rumelhart et al., 1986; Nykänen, 2008) was utilized to tune the parameters of the network. In backward propagation, the training outcomes of the neural network parameters are defined by the election of a proper objective function. The mean square error (MSE) was considered as the objective function in the training process of the model in this study. The MSE can be described as follows:

$$MSE = \frac{1}{n} \sum_{i=1}^n (Y - \hat{Y})^2 \quad (1)$$

where  $\hat{Y}$  is the predicted output,  $Y$  is the target output, and  $n$  indicates the number of samples. After computing the gradient for all the parameters of the model, the gradient descent algorithm was applied to update the parameters as follows (Li et al., 2012; Candel and LeDell,

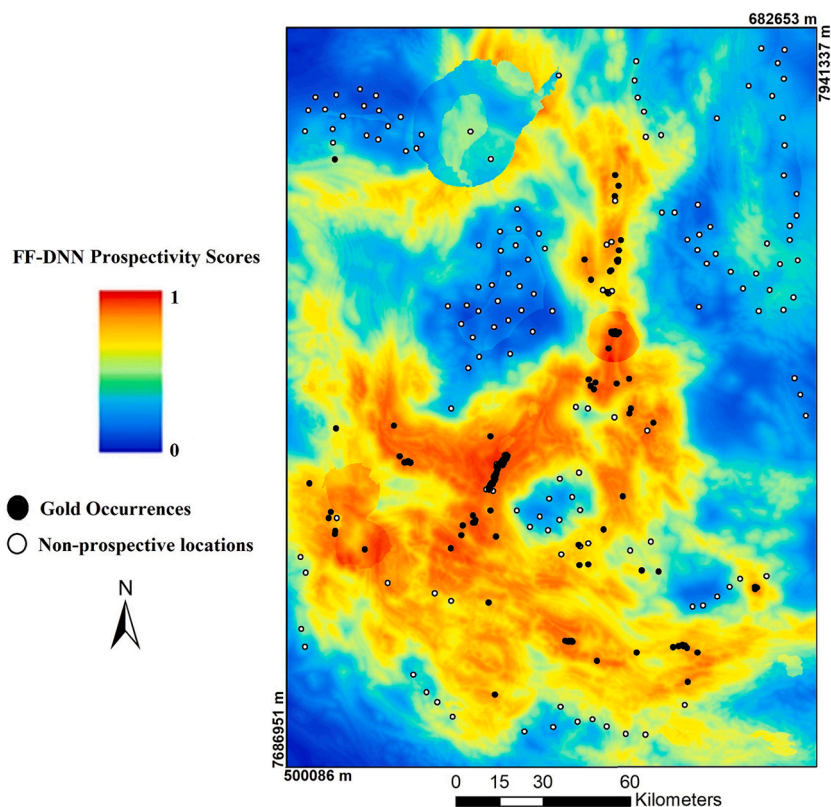


Fig. 17. FF-DNN potential map generated by combining the 19 competent predictor maps.

2022):

$$\theta^{(l)}(t+1) = \theta^{(l)}(t) - \alpha \frac{\partial \text{MSE}}{\partial \theta^{(l)}} \quad (2)$$

In the above equation,  $\theta^{(l)} = \{W, B\}$ , where  $B$  is the bias vector,  $W$  is the weight matrix, and  $l$  denotes the layer number, and  $t$  is the iteration count. In addition,  $\alpha$  ( $0 < \alpha < 1$ ) is the learning rate that controls the step sizes during gradient descent. Neurons should be activated through an activation function in order to introduce intricate features into the neural network. Hyperbolic tangent, sigmoid, and rectified linear unit (ReLU) are examples of activation functions. In this study, the ReLU function that is non-supersaturated and partially linear (Fig. 3) was utilized to easily train and to achieve better performance. The ReLU can be described as follows:

$$f(x) = \max(0, x) \quad (3)$$

Unlike the hyperbolic tangent and sigmoid activation functions, the activation function of ReLU allows models to perform better and learn faster by overcoming the vanishing gradient problem (Basodi et al., 2020). It should be noted that the learning rate should not be set too large if the neuron in which ReLU is placed receives an exceedingly large gradient data stream. This is because the neuron may no longer reflect any input data (Xu et al., 2021). To reduce the overfitting, termed overtraining, in the training process of the model, we utilized the dropout procedure, which randomly selects  $p\%$  of neurons whose gradients will not be updated in the current iteration. In other words, this procedure can randomly impress the nodes of hidden layers to lose power in the training phase as illustrated in Fig. 4, but their weights are intact. In addition, the nodes are able to resume their activity when a new sample is input (Srivastava et al., 2014).

#### 4.1. Results and discussion

##### 4.1.1. Generation of FIS mineral potential model

Fuzzy inference systems (FIS) present a knowledge-driven approach that has been effectively used in MPM (Porwal et al., 2015; Chudasama et al., 2016; Barak et al., 2020) due to the technique offering certain advantages: it (i) avoids direct assignment of weights to spatial proxies (i.e., predictor maps), the weights are estimated via objective functions, (ii) uses natural language and linguistic variables, which is the biggest advantage because an exploration expert can intuitively relate to the system, (iii) offers a framework for predictive modelling of the mineral systems components using spatial proxies in a consistent, yet flexible way, (iv) can be easily implemented using the fuzzy logic tool box of MATLAB™ as well as the model builder and map algebra tools provided in the Spatial Analyst tool box of ArcGIS™, (v) can be effectively used in both brownfields and greenfields areas as it does not require known mineral occurrences as training data, and (vi) avoids the over-fitting problem since the known data distribution is not at all used in estimating prospectivity (Porwal et al., 2015).

A two-phase FIS was utilized in this study (Fig. 5), capable of combining the various exploration predictor maps representing the mappable processes of orogenic gold systems in the GTO (Table 1). During the first phase, individual FIS were developed for each of the pivotal components, including metallogenic trends, lower crustal pathways, upper crustal pathways, structural preparations, lithological preparations, and depositions. In the second phase, a conjunction operator was applied to combine the outputs of each of the individual FIS.

It is possible to determine the efficacy of the output and input variables on the targeted mineralization. For this, we utilized piece-wise linear functions to allocate fuzzy membership scores to the output and input variables (Fig. 6b and 7 Electronic Supplementary Material, Items 1–3). In addition, we applied the C-A plots to interpret how the geological features affect the targeted mineralization (Fig. 6a and



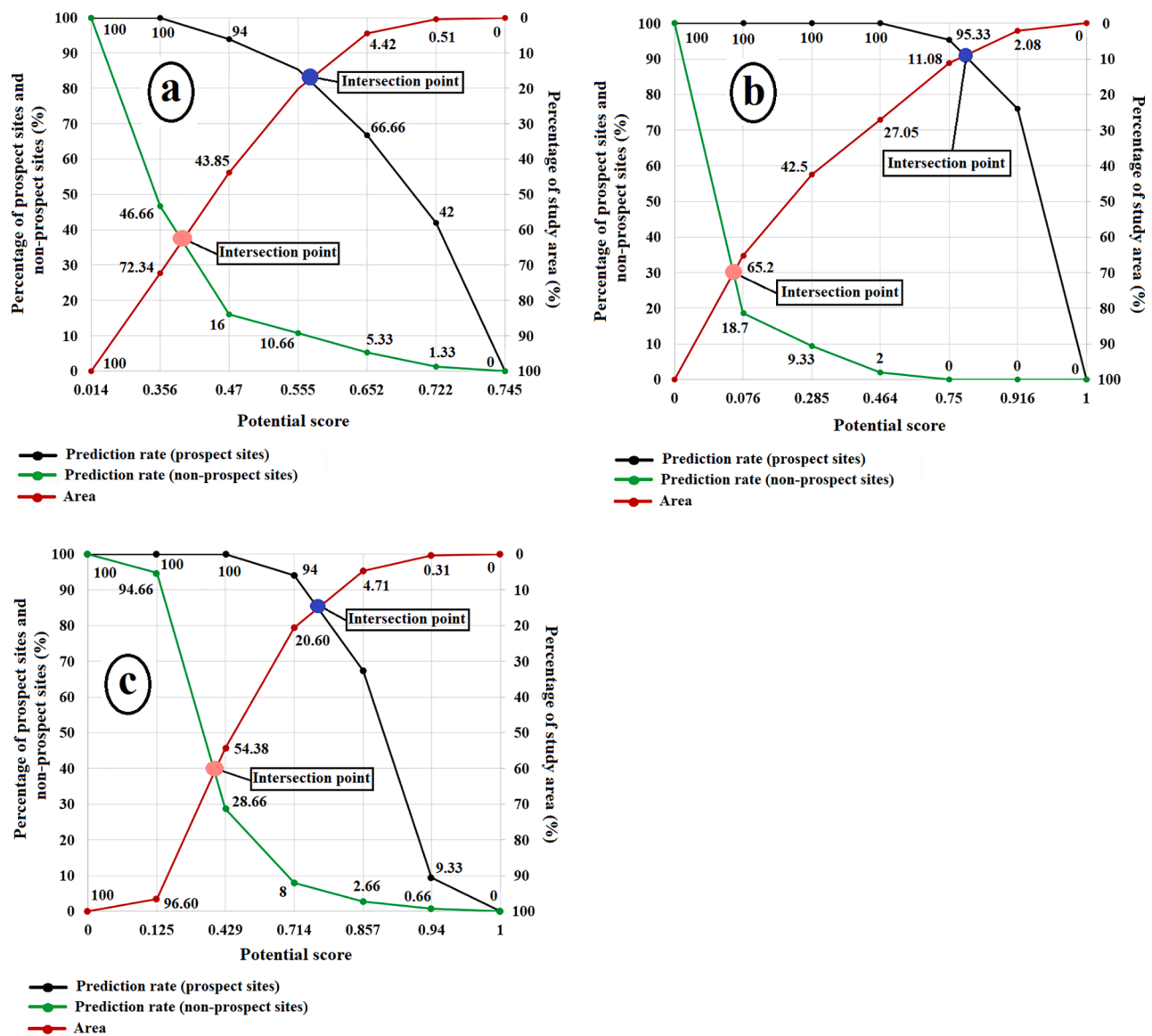


Fig. 18. Improved prediction-area plot for the potential models of (a) fuzzy inference systems, (b) RF generated with the 19 normalized competent predictor maps and (c) feed-forward deep neural network.

Table 4

Extracted parameters from improved prediction-area plots for the targeting models.

	FIS potential model	RF potential model	FF-DNN potential model
$P_m$ (Hits)	83	92	86
$P_n$ (False alarms)	37	30	39
$100 - P_m$ (Misses)	17	8	14
$100 - P_n$ (Correct rejection)	63	60	61
True positive rate ( $TP_r$ )	0.83	0.92	0.86
False positive rate ( $FP_r$ )	0.37	0.3	0.39
$O_p$	0.46	0.62	0.47

Electronic Supplementary Material, Items 4–6). For example, as is commonly done in MPM, we devised a series of buffer zones around the major faults defining interpreted zones of influence within which the wall rocks are interpreted to have been affected by fault activity and fluid-rock interaction. More specifically, we assumed that at distances (i)

between 0 m and 1538 m deformation and fluid flow along the major faults almost certainly affected the surrounding rock volume, (ii) between 1538 m and 26719 m the efficacy of the major faults declined in a linear fashion away from these structures, and (iii) beyond 26719 m the major faults almost certainly did not affect the surrounding rock volume. This concept is incorporated in the piece-wise linear fuzzy membership function for the linguistic value “proximal” (Fig. 6b, curve a).

The linguistic values applied to define the membership functions are listed in Table 2. To analyse the potential of each ground unit area for gold mineralization, several ‘if-then’ rules were developed on the basis of orogenic gold mineralization’s generalized geological settings and our knowledge of orogenic gold mineral systems in the GTO (Fig. 8 and Electronic Supplementary Material, Items 7–12). The rules were embedded in the FIS to predict the possibilities of the targeted mineral occurrences in the ground unit area and thereby allocate potential scores on a fuzzy scale ranging from 0 to 1, with one being prospective and zero being non-prospective (Chudasama et al., 2016). The rules, for example, applied to designing the metallogenic trends FIS are listed in Table 3. The values of the input variables are appraised by the ‘if’ portion of the rules, and the prospectivity for each component is created in the ‘then’

portion. In this study, the ‘if-then’ rules were combined through the MIN implication operator, and then the MAX aggregation operator was utilized to combine the ‘then’ part of the rules. The centroid technique was finally applied to calculate the final potential value for each of the pivotal components. This led to the generation of six intermediate predictor maps that indicate the potential for each of the pivotal components: metallogenic trends, lower crustal pathways, upper crustal pathways, structural preparations, lithological preparations, and depositions.

The following stage involved combination of all six FIS to generate the final mineral potential model. To achieve this, the output maps of metallogenic trends, lower crustal pathways, and upper crustal pathways were integrated through an ‘OR’ operator to develop a single map indicating potential scores for transports (Fig. 9). Also, an ‘OR’ operator was used to integrate the output maps of structural preparations and lithological preparations to generate a single map that shows potential scores for traps (Fig. 10). Ultimately, the ‘PRODUCT’ operator was applied to combine the potential maps of transports (Fig. 9), traps (Fig. 10), and depositions (Fig. 11) to generate the ultimate fuzzy potential model for gold deposits in the study area (Fig. 12).

#### 4.1.2. Generation of RF mineral potential model

Roshanravan et al. (2020) generated an RF potential map of gold potential in the GTO by applying the original (non-transformed) competent predictor maps listed in Table 1. In this study, and for the purpose of comparison, we examined how normalized (transformed) predictor maps may influence the RF modelling outcome. To achieve this, we normalized the same predictor maps through the following equation (Bishop, 1997):

$$X_i = \frac{x_i - x_{\min}}{x_{\max} - x_{\min}} \quad (4)$$

where  $x_{\min}$  and  $x_{\max}$  are the smallest and largest indicator values pertaining to  $i^{\text{th}}$  predictor map, respectively,  $x_i$  is the indicator value for the cell of the  $i^{\text{th}}$  input map, and  $X_i$  for per cell is the normalized score of the indicator value. Thus, predictor map indicator values fall within a range of [0, 1]. Here, we utilized training data comprised of 150 prospect sites (i.e., gold deposits and occurrences, significant mineralized drill intercepts) and 150 non-prospect sites as previously defined by Roshanravan et al. (2020). Non-prospect sites were selected pursuant to the following rules: (i) They ought to be outside the gold permissive tract, (ii) they ought to be distant from the prospect sites, and (iii) their spatial distribution ought to be random.

After normalizing the 19 competent predictor maps, an  $m$  value of 7 and  $n$  value of 1000 were selected in accordance with the procedure provided by Rodriguez-Galiano et al. (2014). Fig. 13 illustrates the important of the predictor variables in the RF modelling based on the mean decrease in the accuracy and Gini impurity index. According to this figure, the proximity to compositionally heterogeneous rock packages is the most significant predictor map in this study while the proximity to gravity worms, based on the  $M_a$ , and the domains of greater fault density, based on the  $M_G$ , are the least significant ones. Fig. 14 indicates the ultimate RF potential model generated via the normalized spatial proxies with the training error curve illustrated in Fig. 15. According to the latter, the error rate of modelling progressively decreases when the number of decision trees rises, with an MSE value of approximately 0.13 for the first decision tree and 0.065 for the 1,000th iteration.

#### 4.1.3. Generation of deep neural network mineral potential model

Here, we applied a supervised feed-forward deep neural network (FF-DNN) to model gold potential pursuant to the following steps:

- Data preprocessing: For the purpose of training and evaluation, the FF-DNN, like any other machine learning approach, requires access to training data. Because the varied scaling of the indicator values of

the predictor maps makes it more difficult to train the model, the indicator values were first normalized using Eq. (4) to reduce variability, thereby generating a more restricted range of values.

- Partitioning of training data: Training of the FF-DNN requires both non-prospect and prospect sites. Here, we utilized the training data previously defined by Roshanravan et al. (2020) with the non-prospect and prospect sites randomly partitioned into testing and training data at a ratio of 20:80. Whilst the training data were used to tune the weights of the network, the testing data were utilized to appraise the generalization efficiency of the trained FF-DNN when new data are processed.
- Selection of the best network: As a next step, the values of the gridded predictor maps were combined to develop an input feature vector for each cell unit [0.04 km<sup>2</sup>] of the study area. In addition, binary coding, (i.e., the assignment of values between 0 and 1) of non-prospect and prospect sites was applied to every single output node. To determine the best network, we randomly performed the FF-DNN with various numbers of hidden layers and nodes. The initial weights were stored for each of the training networks and then utilized to generalize the testing dataset. Finally, the best performing network rendering the least MSE with respect to the testing data could be identified and selected (Fig. 16). It should be noted that the dropout rate was experimentally considered to be 10 % to reduce the overfitting problem.
- Prediction: The best network (i.e., network 12: Fig. 16) was then applied to process the input feature vectors for the entire gridded study area, generating the orogenic gold targeting model for the study area (Fig. 17).

For the purpose of this study, we performed the FF-DNN modelling in the R environment using the default hyperparameters of the h2o package. Ideally, for the FF-DNN network to work most efficiently, its hyperparameters should be adjusted and more training samples should be generated using a variety of data augmentation methods. However, as demonstrated by Sun et al. (2020), a well-performing deep neural network can be created using as little as 118 prospect sites and without any data augmentation. Given the exploratory nature of our FF-DNN modelling and findings of Sun et al. (2020), we followed a similar approach in this study.

#### 4.1.4. Comparison of mineral potential models

After having generated three different gold potential models (Figs. 12, 14 and 17), the training data of Roshanravan et al. (2020) were utilized as control points to appraise model performance. As part of this step, the improved prediction-area (P-A) plot procedure of Roshanravan et al. (2019) was applied. Unlike other validation procedures such as standard prediction area plots (e.g., Roshanravan et al., 2018), receiver operating characteristics curves (e.g., Chen, 2015; Nykänen et al., 2015) and success-rate and prediction-rate curves (e.g., Chung and Fabbri, 2003), the improved P-A plot has the ability to reliably and simultaneously evaluate three pivotal parameters, namely the (i) occupied area of modelled exploration targets, (ii) prediction rate of non-prospect sites, and (iii) prediction rate of prospect sites. As depicted by the improved P-A plots in Fig. 18 and the efficiency statistics summarized in Table 4, the overall performance,  $O_p$ , of the RF potential map generated with the transformed predictor maps is 0.62. As such, it boasts a higher performance value than any of the data-driven (i.e., non-transformed predictor maps-based RF and COA-SVR) and continuous (i.e., data-driven index overlay, geometric average, and fuzzy gamma) mineral potential models previously generated by Roshanravan et al. (2020), using the same study area, targeting model and predictor maps.

Although FIS is a knowledge-driven method based on expert opinion (Porwal et al., 2015), its performance is similar to that of the geometric average method, a continuous, so-called ‘fourth generation’ MPM method. However, computationally, the latter method is much faster than the former. The RF-generated gold potential map, which utilizes

transformed predictor maps, performed best among the eight GTO gold potential maps developed by Roshanravan et al. (2020, 2021, this study) to date. Whilst the COA-SVM potential map performed better than the RF potential map, the former was generated using the original, non-transformed predictor maps. This result illustrates the positive effect of employing transformed predictor maps with respect to RF model performance. It should be noted that although we performed the FF-DNN model without adjusting hyperparameters and data augmentation, its performance was better than that of any of the continuous (i.e., geometric average, data-driven index overlay and fuzzy gamma) and knowledge-driven (i.e., FIS) models generated by Roshanravan et al. (2020) and in this study.

## 5. Summary and conclusions

In this study, we adopted a multi-technique approach to MPM, using Mamdani-type fuzzy inference system (FIS), feed-forward deep neural network (FF-DNN) and transformed predictor map-based random forest (RF) methods to (i) model orogenic gold potential in the Granites-Tanami Orogen (GTO) in Australia's Northern Territory, and (ii) compare the performance of these models to those previously generated for the same study area and using the same targeting model and predictor maps.

Our assessment of model efficiency demonstrated that the transformed predictor map-based RF method performed best amongst the eight models generated thus far. More specifically, the transformed predictor map-based RF method achieved a superior overall performance index ( $O_p$ ) value of 0.62 compared to the FF-DNN ( $O_p = 0.47$ ) and FIS ( $O_p = 0.46$ ) approaches. In addition, the transformed predictor map-based RF model was found to be superior to the data-driven, non-transformed predictor map-based RF ( $O_p = 0.49$ ) and COA-SVR ( $O_p = 0.54$ ) as well as the continuous, geometric average ( $O_p = 0.46$ ), data-driven index overlay ( $O_p = 0.45$ ) and fuzzy gamma ( $O_p = 0.45$ ) models of Roshanravan et al. (2020, 2021). The assessment results, thus, clearly indicate the positive effect of applying transformed predictor maps with respect to RF model performance.

Overall, our multi-technique approach to MPM and the comparing and contrasting of a large set of resulting gold potential models, offered (i) insights that cannot be derived from a single MPM technique and were critical in the development and calibration of new tools and techniques described in this paper, and (ii) what we believe are more robust gold exploration targets. As a result, we strongly recommend using a multi-technique approach to MPM, which we hope will soon replace the currently accepted and widely utilized single-technique approach.

## Declaration of Competing Interest

The authors declare that they have no known competing financial interests or personal relationships that could have appeared to influence the work reported in this paper.

## Data availability

Data will be made available on request.

## Acknowledgments

The authors are grateful to Prodigy Gold NL for providing access to personnel and data, and permission to publish this work. In addition, we would like to sincerely thank the Associate Editor Dr. Daniel Müller for his expert handling of this paper. Furthermore, we would like to express our immense gratitude to two anonymous reviewers who provided insightful feedback and remarks that helped to significantly increase the quality of our submission.

## Appendix A. Supplementary data

Supplementary data to this article can be found online at <https://doi.org/10.1016/j.oregeorev.2022.105224>.

## References

- Ahmad, M., Vandenberg, L. C., Wygralak, A. S., 2013. Chapter 11: Tanami Region. In: Ahmad, M., Munson T. J. [Compilers], *Geology and mineral resources of the Northern Territory*. Northern Territory Geological Survey, Special Publication 5, 11: 1–11:41.
- Aryafar, A., Roshanravan, B., 2021. BWM-SAW: a new hybrid MCDM technique for modeling of chromite potential in the Birjand district, east of Iran. *J. Geochem. Explor.* 231, 106876.
- Australia's Mining Monthly, 2020. The Chalice story. Available online at: <https://www.miningmonthly.com/advancing-exploration/opinion/1386321/the-chalice-story> [last accessed on 25 September 2022].
- Bagas, L., 2010. Evolution and tectonic setting of the Paleoproterozoic Granites-Tanami Orogen, Western Australia. The University of Western Australia, p. 280. Unpublished PhD Thesis.
- Bagas, L., Bierlein, F.P., English, L., Anderson, J.A., Maidment, D., Huston, D.L., 2008. An example of a Palaeoproterozoic back-arc basin: Petrology and geochemistry of the ca. 1864 Ma Stubbins Formation as an aid towards an improved understanding of the Granites-Tanami Orogen, Western Australia. *Precamb. Res.* 166, 168–184.
- Bagas, L., Bierlein, F.P., Anderson, J.A.C., Maas, R., 2010. Collision-related granitic magmatism in the Granites-Tanami Orogen, Western Australia. *Precamb. Res.* 177, 212–226.
- Bagas, L., Boucher, R., Li, B., Miller, J., Hill, P., Depauw, G., Pascoe, J., Eggers, B., 2014. Paleoproterozoic stratigraphy and gold mineralisation in the Granites-Tanami Orogen, North Australian Craton. *Aust. J. Earth Sci.* 61, 89–111.
- Baggott, M., Schneider, S., Robinson, C., 2016. Exploration success and resource growth at Newmont's Tanami operations, Northern Territory. AGES 2016, Northern Territory Geological Survey Annual Geoscience Exploration Seminar, Alice Springs, 15–16 March 2016, 24 p.
- Barak, S., Abedi, M., Bahrudi, A., 2020. A knowledge-guided fuzzy inference approach for integrating geophysics, geochemistry, and geology data in a deposit-scale porphyry copper targeting, Saveh, Iran. *Bollettino di Geofisica Teorica ed Applicata* 61 (2).
- Basodi, S., Ji, C., Zhang, H., Pan, Y., 2020. Gradient amplification: An efficient way to train deep neural networks. *Big Data Mining and Analytics* 3, 196–207.
- Behara, S., Panigrahi, M.K., 2022. Gold prospectivity mapping and exploration targeting in Hutti-Maski schist belt, India: synergistic application of Weights-of-Evidence (WOE), Fuzzy Logic (FL) and hybrid (WOE-FL) models. *J. Geochem. Explor.* 235, 106963.
- Bengio, Y., 2009. Learning Deep Architectures for AI. *Foundations and Trends®. Mach. Learn.* 2, 1–127.
- Betts, P.G., Armit, R.J., Stewart, J., Aitken, A.R.A., Ailleres, L., Donchak, P., Hutton, L., Withnall, I., Giles, D., 2016. Australia and Nuna. *Geol. Soc. Lond. Spec. Publ.* 424, 47–81.
- Bishop, C.M., 1997. *Neural Networks for pattern recognition*. Oxford University Press.
- Bonham-Carter, G.F., 1994. *Geographic Information Systems for Geoscientists: Modelling With GIS*. Pergamon, Oxford.
- Breiman, L., 2001. Random forests. *Mach. Learn.* 45, 5–32.
- Candel, A., LeDell, E., 2022. Deep learning with H2O. Sixth Edition 1–55.
- Carranza, E.J.M., 2008. Geochemical anomaly and mineral prospectivity mapping in GIS. *Handbook of Exploration and Environmental Geochemistry*, Elsevier, Amsterdam, 11, 351 pp.
- Carranza, E.J.M., Laborte, A.G., 2015. Random forest predictive modeling of mineral prospectivity with small number of prospects and data with missing values in Abra (Philippines). *Comput. Geosci.* 74, 60–70.
- Cawood, P.A., Korsch, R.J., 2008. Assembling Australia: Proterozoic building of a continent. *Precamb. Res.* 166, 1–38.
- Chalice Mining Limited, 2020. Significant nickel-palladium discovery confirmed at Julimar. Australian Securities Exchange Announcement, 15 April 2020. Available from: <https://chalicemining.com/sites/default/files/asx-announcements/02224944.pdf>.
- Chalice Mining Limited, 2021. Tier-1 scale maiden Mineral Resource for Gonneville – 10Moz Pd+Pt+Au (3E), 530kt Ni, 330kt Cu and 53kt Co. Australian Securities Exchange Announcement, 09 November 2021. Available from: <https://chalicemining.com/sites/default/files/asx-announcements/61061655.pdf>.
- Chen, Y., 2015. Mineral potential mapping with a restricted Boltzmann machine. *Ore Geol. Rev.* 71, 749–760.
- Cheng, Q., Agterberg, F.P., Ballantyne, S.B., 1994. The separation of geochemical anomalies from background by fractal methods. *J. Geochem. Explor.* 51, 109–130.
- Chudasama, B., Kreuzer, O.P., Thakur, S., Porwal, A.K., Buckingham, A.J., 2018. Surficial uranium mineral systems in Western Australia: Geologically-permissive tracts and undiscovered endowment. In: Quantitative and spatial evaluations of undiscovered uranium resources. International Atomic Energy Agency, IAEA-TECDOC-1861, 446–614.
- Chudasama, B., Porwal, A., Kreuzer, O.P., Butera, K., 2016. Geology, geodynamics and orogenic gold prospectivity modelling of the Paleoproterozoic Kumasi Basin, Ghana, West Africa. *Ore Geol. Rev.* 78, 692–711.
- Chung, C.J.F., Fabbri, A.G., 2003. Validation of spatial prediction models for landslide hazard mapping. *Nat. Hazards* 30, 451–472.



- Crispe, A.J., Vandenberg, L.C., Scrimgeour, I.R., 2007. Geological framework of the Archean and Paleoproterozoic Tanami Region, Northern Territory. *Miner. Depos.* 42, 3–26.
- Daviran, M., Maghsoudi, A., Ghezlbash, R., Pradhan, B., 2021. A new strategy for spatial predictive mapping of mineral prospectivity: Automated hyperparameter tuning of random forest approach. *Comput. Geosci.* 148, 104688.
- Dietterich, T.G., 2002. Ensemble learning. *The Handbook of Brain Theory and Neural Networks* 2, 110–125.
- Dulfer, H., Milligan, P.R., Coghlan, R., Czarnota, K., Highet, L.M., Champion, D.C., Skirrow, R.G., 2016. Potential for intrusion-hosted Ni-Cu-PGE sulfide deposits in Australia: a continental-scale analysis of mineral system prospectivity. *Geosci. Austr.*
- Ford, A., 2020. Practical implementation of random forest-based mineral potential mapping for porphyry Cu–Au mineralization in the Eastern Lachlan Orogen, NSW, Australia. *Nat. Resour. Res.* 29, 267–283.
- Glorot, X., Bengio, Y., 2010. Understanding the difficulty of training deep feedforward neural networks. In *Proceedings of the thirteenth international conference on artificial intelligence and statistics* (pp. 249–256). JMLR Workshop and Conference Proceedings.
- Goodfellow, I., Bengio, Y., Courville, A., 2016. Deep learning. MIT press.
- Hronsky, J.M., Kreuzer, O.P., 2019. Applying spatial prospectivity mapping to exploration targeting: fundamental practical issues and suggested solutions for the future. *Ore Geol. Rev.* 107, 647–653.
- Huston, D.L., Vandenberg, L., Wygralak, A.S., Mernagh, T.P., Bagas, L., Crispe, A., Lambeck, A., Cross, A., Fraser, G., Williams, N., Worden, K., 2007. Lode-gold mineralization in the Tanami region, northern Australia. *Miner. Depos.* 42, 175–204.
- Joly, A., McCuaig, T.C., Bagas, L., 2010. The importance of early crustal architecture for subsequent basin-forming, magmatic and fluid flow events The Granites-Tanami Orogen example. *Precamb. Res.* 182, 15–29.
- Joly, A., Porwal, A., McCuaig, T.C., 2012. Exploration targeting for orogenic gold deposits in the Granites-Tanami Orogen: mineral system analysis, targeting model and prospectivity analysis. *Ore Geol. Rev.* 48, 349–383.
- Keykhay-Hosseinpoor, M., Kohsary, A.H., Hossein-Morshedy, A., Porwal, A., 2020. A machine learning-based approach to exploration targeting of porphyry Cu–Au deposits in the Dehsalm district, eastern Iran. *Ore Geol. Rev.* 116, 103234.
- Kreuzer, O.P., Etheridge, M.A., Guj, P., McMahon, M.E., Holden, D.J., 2008. Linking mineral deposit models to quantitative risk analysis and decision-making in exploration. *Econ. Geol.* 103, 829–850.
- Kreuzer, O.P., Buckingham, A., Mortimer, J., Walker, G., Wilde, A., Appiah, K., 2019. An integrated approach to the search for gold in a mature, data-rich brownfields environment: a case study from Sigma-Lamaque. *Quebec. Ore Geology Rev.* 111, 102977.
- Kreuzer, O.P., Yousefi, M., Nykänen, V., 2020. Introduction to the special issue on spatial modelling and analysis of ore-forming processes in mineral exploration targeting. *Ore Geol. Rev.* 119, 103391.
- LeCun, Y., Bengio, Y., Hinton, G., 2015. Deep learning. *nature*, 521, 436–444.
- Li, B., Bagas, L., Jourdan, F., 2014. Tectono-thermal evolution of the Palaeoproterozoic Granites-Tanami Orogen, North Australian Craton: implications from hornblende and biotite 40Ar/39Ar geochronology. *Lithos* 206, 262–276.
- Li, J., Cheng, J.H., Shi, J.Y., Huang, P., 2012. In: *Brief Introduction of Back Propagation (BP) Neural Network Algorithm and Its Improvement*. Springer, Berlin, Heidelberg, pp. 553–558.
- Maepa, F., Smith, R.S., Tessema, A., 2021. Support vector machine and artificial neural network modelling of orogenic gold prospectivity mapping in the Swayze greenstone belt, Ontario, Canada. *Ore Geol. Rev.* 130, 103968.
- Maidment, D. W., Wingate, M. T. D., Clauoué-Long, J. C., Bodorkos, S., Huston, D. L., Whelan, J. A., Bagas, L., Lambeck, A., Lu, Y., 2020. Geochronology of metasedimentary and granitic rocks in the Granites-Tanami Orogen: 1885–1790 Ma geodynamic evolution. *Geological Survey of Western Australia, Report* 196, 50 p.
- McCuaig, T.C., Beresford, S., Hronsky, J., 2010. Translating the mineral systems approach into an effective exploration targeting system. *Ore Geol. Rev.* 38, 128–138.
- Nykanen, V., 2008. Radial basis functional link nets used as a prospectivity mapping tool for orogenic gold deposits within the Central Lapland Greenstone Belt, Northern Fennoscandian Shield. *Nat. Resour. Res.* 17, 29–48.
- Nykanen, V., Lahti, I., Niiranen, T., Korhonen, K., 2015. Receiver operating characteristics (ROC) as validation tool for prospectivity models—A magmatic Ni–Cu case study from the Central Lapland Greenstone Belt, Northern Finland. *Ore Geol. Rev.* 71, 853–860.
- Parsa, M., 2021. A data augmentation approach to XGboost-based mineral potential mapping: an example of carbonate-hosted ZnPb mineral systems of Western Iran. *J. Geochem. Explor.* 228, 106811.
- Parsa, M., Carranza, E.J.M., Ahmadi, B., 2022. Deep GMDH neural networks for predictive mapping of mineral prospectivity in terrains hosting few but large mineral deposits. *Nat. Resour. Res.* 31 (1), 37–50.
- Parsa, M., Maghsoudi, A., 2021. Assessing the effects of mineral systems-derived exploration targeting criteria for Random Forests-based predictive mapping of mineral prospectivity in Ahar-Arasbaran area, Iran. *Ore Geol. Rev.* 138, 104399.
- Petrella, L., Thébaud, N., LaFlamme, C., Miller, J., McFarlane, C., Occhipinti, S., Turner, S., Perazzo, S., 2020. Contemporaneous formation of vein-hosted and stratabound gold mineralization at the world-class Dead Bullock Soak mining camp, Australia. *Miner. Depos.* 55 (5), 845–862.
- Porwal, A., Das, R.D., Chaudhary, B., Gonzalez-Alvarez, I., Kreuzer, O., 2015. Fuzzy inference systems for prospectivity modeling of mineral systems and a case-study for prospectivity mapping of surficial Uranium in Yeelirrie Area, Western Australia. *Ore Geol. Rev.* 71, 839–852.
- Porwal, A.K., Kreuzer, O.P., 2010. Introduction to the special issue: mineral prospectivity analysis and quantitative resource estimation. *Ore Geol. Rev.* 38, 121–127.
- Rodriguez-Galiano, V.F., Chica-Olmo, M., Chica-Rivas, M., 2014. Predictive modelling of gold potential with the integration of multisource information based on random forest: a case study on the Rodalquilar area, Southern Spain. *Int. J. Geogr. Inf. Sci.* 28, 1336–1354.
- Rodriguez-Galiano, V., Sanchez-Castillo, M., Chica-Olmo, M., Chica-Rivas, M., J.O.G.R., 2015. Machine learning predictive models for mineral prospectivity: An evaluation of neural networks, random forest, regression trees and support vector machines. *Ore Geol. Rev.* 71, 804–818.
- Roshanravan, B., 2020. Translating a mineral systems model into continuous and data-driven targeting models: an example from the Dolatabad Chromite District, Southeastern Iran. *J. Geochem. Explor.* 215, 106556.
- Roshanravan, B., Agajani, H., Yousefi, M., Kreuzer, O., 2018. Generation of a geochemical model to prospect podiform chromite deposits in North of Iran. In: *In 80th EAGE Conference and Exhibition 2018*, Vol. 2018(1. European Association of Geoscientists & Engineers, pp. 1–5.
- Roshanravan, B., Aghajani, H., Yousefi, M., Kreuzer, O., 2019. An improved prediction-area plot for prospectivity analysis of mineral deposits. *Nat. Resour. Res.* 28, 1089–1105.
- Roshanravan, B., Kreuzer, O.P., Bruce, M., Davis, J., Briggs, M., 2020. Modelling gold potential in the Granites-Tanami Orogen, NT, Australia: a comparative study using continuous and data-driven techniques. *Ore Geol. Rev.* 125, 103661.
- Roshanravan, B., Kreuzer, O.P., Mohammadi, S., Bruce, M., Davis, J., Briggs, M., 2021. Cuckoo optimization algorithm for support vector regression potential analysis: an example from the Granites-Tanami Orogen, Australia. *J. Geochem. Explor.* 230, 106858.
- Rumelhart, D.E., Hinton, G.E., Williams, R.J., 1986. Learning representations by back-propagating errors. *Nature* 323, 533–536.
- Srivastava, N., Hinton, G., Krizhevsky, A., Sutskever, I., Salakhutdinov, R., 2014. Dropout: a simple way to prevent neural networks from overfitting. *The journal of machine learning research* 15, 1929–1958.
- Tessema, A., 2017. Mineral systems analysis and artificial neural network modeling of chromite prospectivity in the Western Limb of the Bushveld Complex, South Africa. *Nat. Resour. Res.* 26, 465–488.
- Wang, J., Zuo, R., Xiong, Y., 2020. Mapping mineral prospectivity via semi-supervised random forest. *Nat. Resour. Res.* 29 (1), 189–202.
- Wyborn, L.A.I., Heinrich, C.A., Jaques, A.L., 1994. Australian Proterozoic mineral systems: essential ingredients and mappable criteria. *AusIMM Publ. Ser.* 5 (94), 109–115.
- Wygralak, A.S., Mernagh, T.P., Huston, D.L., Ahmad, M., 2005. Gold mineral system of the Tanami region (p.90). *Northern Territory Geological Survey Report*, 18.
- Xiang, J., Xiao, K., Carranza, E.J.M., Chen, J., Li, S., 2020. 3D mineral prospectivity mapping with random forests: A case study of Tongling, Anhui, China. *Nat. Resour. Res.* 29 (1), 395–414.
- Xiong, Y., Zuo, R., Carranza, E.J.M., 2018. Mapping mineral prospectivity through big data analytics and a deep learning algorithm. *Ore Geol. Rev.* 102, 811–817.
- Xu, Y., Li, Z., Xie, Z., Cai, H., Niu, P., Liu, H., 2021. Mineral prospectivity mapping by deep learning method in Yawan-Daqiao area, Gansu. *Ore Geol. Rev.* 138, 104316.
- Yang, N., Zhang, Z., Yang, J., Hong, Z., 2022. Applications of data augmentation in mineral prospectivity prediction based on convolutional neural networks. *Comput. Geosci.* 161, 105075.
- Yousefi, M., Kreuzer, O.P., Nykänen, V., Hronsky, J.M., 2019. Exploration information systems—A proposal for the future use of GIS in mineral exploration targeting. *Ore Geol. Rev.* 111, 103005.
- Zadeh, L.A., 1973. Outline of a new approach to the analysis of complex systems and decision processes. *IEEE Trans. Syst. Man Cybern.* 28–44.
- Zhang, S., Carranza, E.J.M., Xiao, K., Wei, H., Yang, F., Chen, Z., Xiang, J., 2021. Mineral prospectivity mapping based on isolation forest and random forest: Implication for the existence of spatial signature of mineralization in outliers. *Nat. Resour. Res.* 1–19.
- Zhou, Z.H., 2016. *Machine Learning*. Tsinghua University Press, Beijing, p. pp., 97 (In Chinese).
- Zuo, R., Kreuzer, O.P., Wang, J., Xiong, Y., Zhang, Z., Wang, Z., 2021. Uncertainties in GIS-based mineral prospectivity mapping: key types, potential impacts and possible solutions. *Nat. Resour. Res.* 30 (5), 3059–3079.